Experimental study on the bearing capacity behaviour of branched piling for stabilisation of constructions on peat: A model investigation

Dinesh K. Jamatia, Ashim K. Dey, Rajat Debnath

Civil Engineering Department, National Institute of Technology Silchar, Assam, India

SUMMARY

Due to rapid population growth, construction on peatlands is inevitable. Peat, as a compressible water-saturated and fibre-rich soil with low strength and unique microstructure, presents significant challenges for construction engineering and requires stabilisation using advanced techniques. Conventionally, piles are generally utilised in locations with thick deposits of weak soils. However, their effectiveness in peat can be limited by excessive settlement, reduced load-bearing capacity, higher construction costs, challenges in achieving lateral stability, and potential for disturbance of the peat layers during installation. To address such limitations, this study introduces the innovative concept of branched piling (BP), in which the piles have branches extending from their outer surfaces. Model scale tests were conducted on branched piles installed in large (approximately 1 m^3) peat samples collected with minimal disturbance from a site at Silchar in the northeast Indian state of Assam. Extensive testing under static loads revealed a 32 % increase in vertical bearing capacity for BP compared to standard piling. Key variables that significantly influenced BP capacity included branch number (n), branch length (L_b) and top branch inclination angle (α). The results showed that increasing n, L_b and α (up to 45°) enhanced capacity, but capacity was reduced if the α value (inclination) exceeded 45°. This new BP technique provides a practical and effective solution for improving stability, load-bearing capacity and durability of foundations on challenging peat deposits. By tackling the challenges of construction on peat, this method bridges the gap between research advancements and practical engineering applications.

KEY WORDS: electrical resistivity, ERT, MASW, model scale tests, settlement, static load

INTRODUCTION

Peat results from incomplete decomposition of plant and animal remains under waterlogged anaerobic conditions, where limited oxygen availability retards breakdown processes. Over millennial timescales, this can lead to the accumulation of a thick layer of partially decomposed organic material (peat) that covers the land, turning it into peatland. Amongst others, regions of the world with tropical climate, high annual rainfall, waterlogged ground, slow-moving rivers, poor drainage and high humidity present favourable conditions for peat formation (Paul *et al.* 2021, Li *et al*. 2020, Debnath *et al.* 2021, Akhtar *et al.* 2022, Wang *et al.* 2023, Sabrekov *et al.* 2023, Tang *et al.* 2024).

Owing to the nature of its formation, peat tends to exhibit high water-absorbing capacity, low bulk density, high organic content (OC), very low strength and significant compressibility, meaning that peatland is challenging ground for construction and infrastructural development. On numerous occasions in the past, construction on peat 'soil' has resulted in catastrophic failures including tilting of buildings, excessive settlement of foundations, cracking or complete collapse of structures, slope instability, road heaving and utility line distortion, leading to frequent maintenance issues. Common failures associated with construction on peatlands are driven by peat's high compressibility, low strength and bearing capacity, and susceptibility to long-term deformation (settlement), as reported in the studies of Debnath *et al.* (2021), Williams-Mounsey *et al.* (2021), Yamazoe *et al.* (2023), Yang *et al*. (2023), Jorat *et al.* (2024), Schneider *et al.* (2024), Yamazoe *et al.* (2025).

Traditionally, construction activities have avoided peatlands because of the challenging soil properties. However, with an exponential surge in population, particularly in recent decades, there is increasing pressure to utilise these (and other) marginal lands for housing, infrastructure and development of paved thoroughfares, despite their complex engineering demands. Therefore, engineers must now address the unique challenges posed by these soils, developing innovative methodologies and techniques to enable safe and sustainable construction on peatlands while minimising environmental impacts.

In this context, numerous attempts have been made in recent decades to enhance the strength of very soft clays or peats by adopting various ground stabilisation methods including incorporation of chemical additives (lime, cement, superabsorbents, rice husk ash, fly ash, etc.) by manual mixing, fibre reinforcement, geosynthetic inclusions, and deep stabilisation techniques such as preloading with vertical drains or electro-osmotic consolidation. Other approaches have involved a variety of pile techniques such as stone columns, sand compaction piles, lime piles, under-reamed piles, squeezed concrete piles, micro piles, helical piles, displacement piles, vibro concrete columns and jet-grouted piles, as detailed in the publications of Paul & Hussain (2020), Khanday *et al.* (2022), Wahab *et al.* (2023), Anuar *et al.* (2024), Bakhir *et al.* (2024), Hassan *et al.* (2024) and Setyaningrum *et al.* (2024). Additionally, vacuum preloading and dynamic compaction have been utilised to further improve load-bearing capacity, reduce settlement and enhance overall ground stability when working with challenging soil conditions.

Despite methodological and technical advances, ground stabilisation methods still face limitations such as environmental impacts, inconsistent load distribution or performance in soft soils, installation complexity, prolonged consolidation, degradation of organic soils, insufficient compaction in very soft soils, lateral soil squeezing, high cost or energy requirements, and potential disturbance to the soil matrix particularly in highly compressible organic soils like peat. Additionally, they may exhibit limited durability under cyclic loading, chemical degradation in aggressive soil environments, quality control difficulties during construction, and challenges in achieving uniform soil improvement across large sites or variable site conditions, as described in the studies of Raut & Verma (2024), Shinde *et al.* (2024) and Tang *et al.* (2024).

The present study aims to overcome these limitations by introducing the concept of branched piling (BP) and testing it under laboratory conditions, although in peat collected from the field. BP was installed in pre-cast moulds within model-scale tanks, to replicate field conditions while minimising major installation challenges such as alignment issues, uneven load distribution, soil disturbance, potential displacement of surrounding soil, inadequate pile penetration, and difficulty in achieving proper compaction around the pile shaft. This controlled setup allowed precise monitoring and analysis which ensured that installation variables were effectively managed to simulate realistic field conditions while reducing common on-site complications.

METHODS

Study material and site

Tropical peat deposits in south and south-east Asia differ significantly from those found in humid temperate regions (Yonebayashi *et al.* 1994, Wüst *et al.* 2008). Climate is a critical factor in the formation of peat, influencing its type, composition and degree of decomposition. These characteristics are further shaped by site-specific elements which include temperature, humidity, persistence of waterlogging, vegetation, ecological system and historical land use.

The peat studied was located on the Elanpur tea (plantation) estate (ETE) in Silchar, a city in the north-east Indian state of Assam (Figure 1). The study area lies on flat terrain characterised by waterlogged conditions. Previous researchers (e.g., Paul *et al*. 2021, Debnath *et al.* 2021) have demonstrated that the climatic conditions are ideal for peat accumulation in this region, where the peatlands are estimated to be between 8,000 and 12,000 years old (Sarangi *et al.* 2022, Debnath *et al.* 2021), reflecting the geological history of the area. The region experiences a tropical monsoon climate, with conditions varying from moderate to humid tropical. Summers are typically long and hot, lasting from March to October. Average annual temperature is approximately 35 °C and influenced by rainfall patterns. Annual rainfall varies between 1922 and 2855 mm, as reported by the Indian Meteorological Department. The southwest monsoon, occurring between April and July, often leads to river flooding.

On-site investigation

A detailed site investigation was carried out by conducting both non-invasive and invasive tests. In the preliminary phase, the non-invasive electrical resistivity test (ERT) and multi-channel analysis of surface waves (MASW) techniques were used to reveal the horizontal and vertical profiles, along with layering detail, of the subsoil (Figure 2, top and middle rows). Detailed descriptions of the ERT and MASW tests are avoided here for reasons of brevity, but may be found by referring to the studies of Saha *et al.* (2022) and Kundu *et al.* (2024). Invasive standard penetration tests (SPT) were also performed according to the international standard IS 2131:1981. This involved boring (auger and wash method) followed by dropping a 65 kg hammer from a height of 75 cm to drive a split spoon sampler into the soil. The number of hammer blows required to penetrate the last 30 cm of a 45 cm drive was recorded as the SPT-*N* value, representing soil resistance to dynamic loading. These values were further corrected to N_{60} to account for energy efficiency. Soil samples for

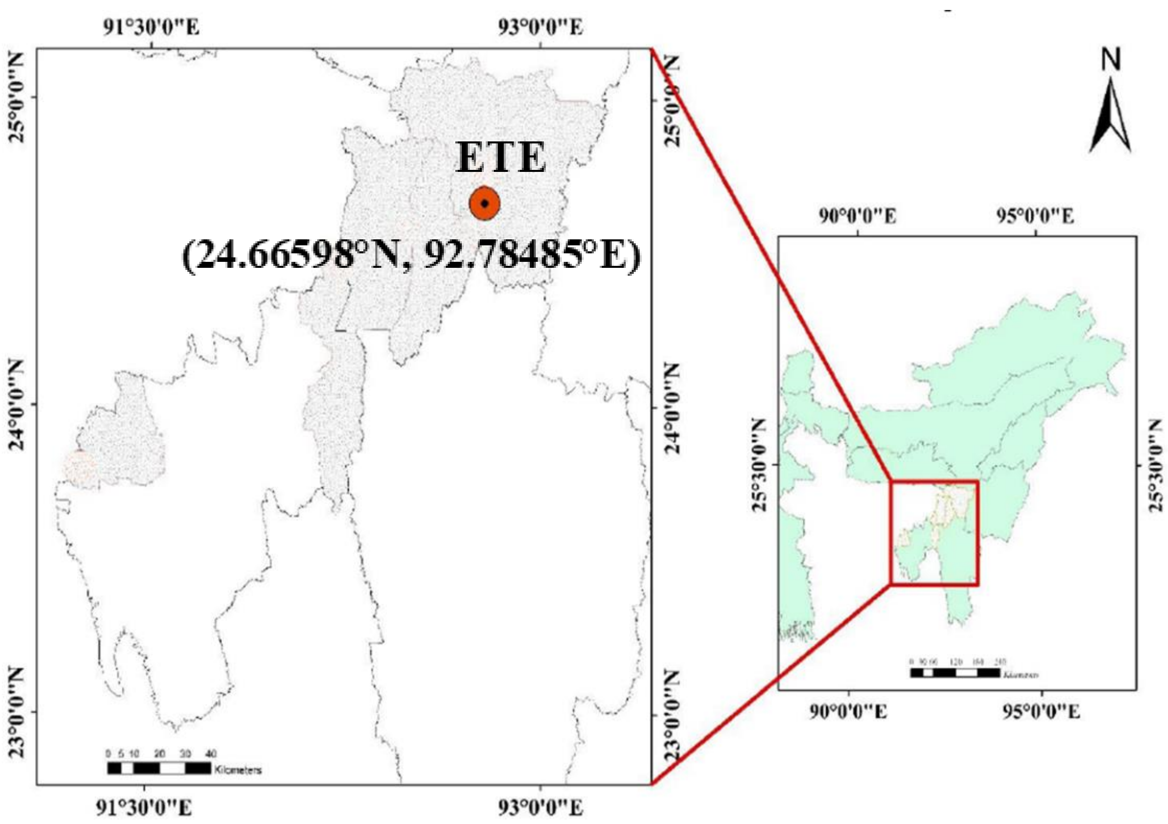

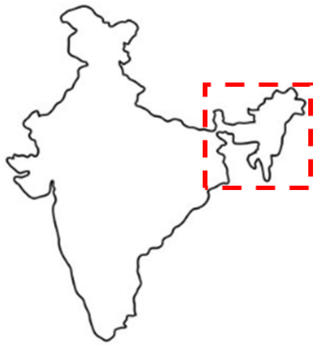

Figure 1. Locations of north-east India (dashed red box on the country outline at bottom right), the study region (solid red box on the map of north-east India at top right), and the study site at Elanpur tea estate (ETE; with red surround and co-ordinates at top left).

laboratory testing were collected during the process, in both disturbed (DS) and undisturbed (UDS) forms (see next sub-section).

Sample collection

As mentioned in the previous sub-section, peat samples were collected during the SPT boring procedure. These samples were used to evaluate physical, microstructural, mineralogical and mechanical properties of the soil by elemental level testing in the laboratory. This integration of field and laboratory data aimed to provide a comprehensive understanding of subsurface characteristics, and thus contribute to the study's geotechnical assessments. DS samples were obtained directly from the split spoon sampler during the SPT tests. UDS samples were carefully (to maintain their natural structure and integrity) extracted from depths ranging from 1.5 m to 6.0 m using Shelby tubes, sealed at both ends with wax, placed in plastic bags, and promptly taped to minimise moisture loss. A photograph showing the location for SPT tests and disturbed-sample (DS) collection (foreground) plus part of the open area covered by UDS sampling (background) is included in Figure 2 (bottom row). After transportation to the laboratory, the UDS samples were stored upright at 20 °C with 85 % humidity.

For the model-scale experiments, additional large (approximately 1 m³) peat samples were carefully extracted from the site by digging pits, as shown in Figure 3(a). The samples were collected with utmost care to preserve their structural integrity, natural composition and in-situ properties, and wrapped securely in polythene sheets to minimise moisture loss and exclude contaminants during handling and transport. They were then transported promptly (within a few hours) to the model-scale experimental facility where they were stored under controlled conditions to prevent degradation or changes in their geotechnical characteristics.

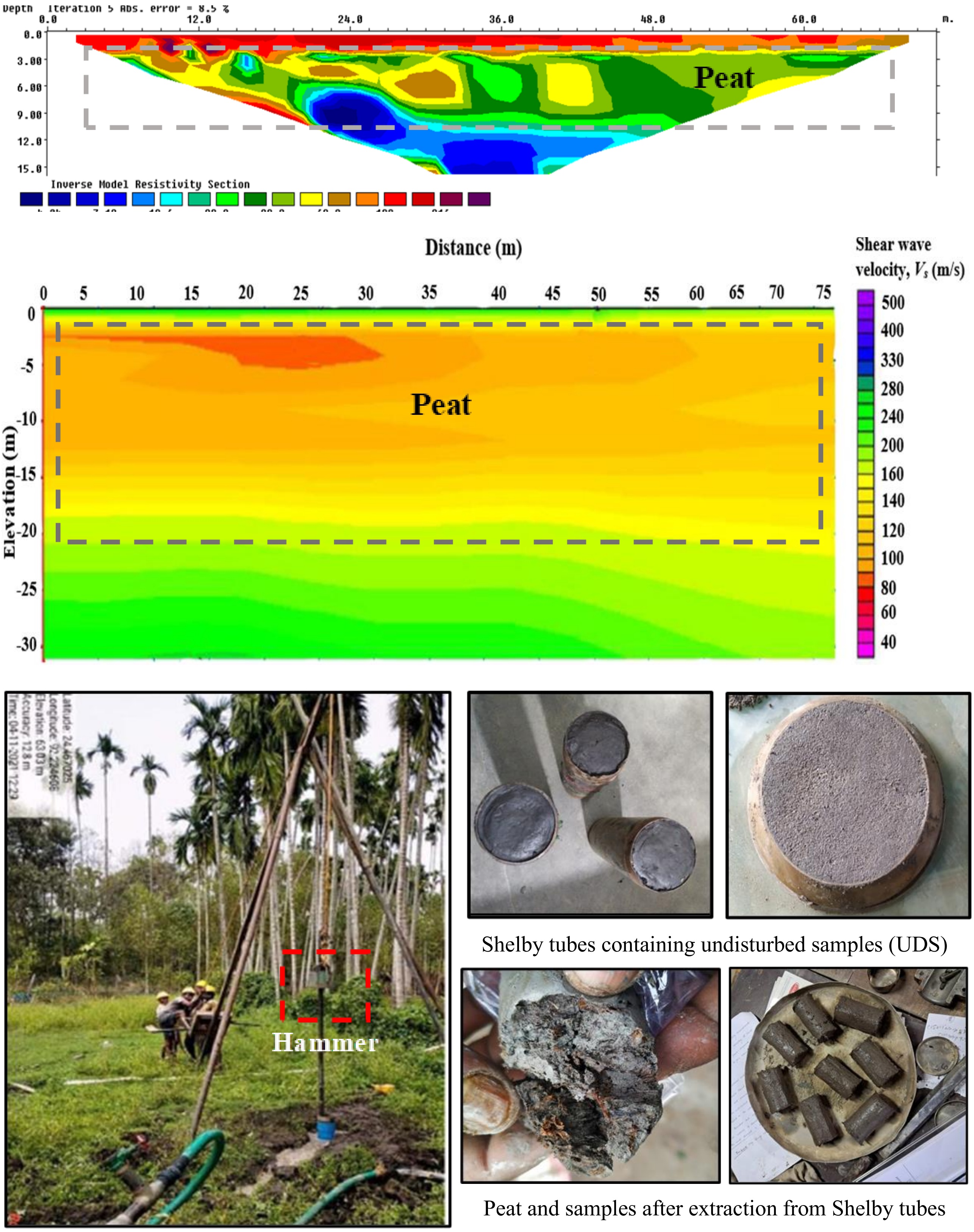

Figure 2. Fieldwork at the ETE site involved two non-invasive test methods, namely: electrical resistivity testing (ERT) (top); and multi-channel analysis of surface waves (MASW) (middle). We also carried out invasive standard penetration testing (SPT; bottom left) which included the collection of peat samples (bottom right). The information gathered enabled key insights about the subsurface soil profile, which contributed to geotechnical characterisation and suitability assessment of the site. See text for further explanation.

(a) (b)

Figure 3. Peat samples were collected from the ETE site to conduct model-scale tests under controlled laboratory conditions. For accurate analysis, representative sampling was ensured by digging out the peat sample from a pit at the test location (a). The model test box (1 m × 1 m) was designed, constructed and prepared to simulate field conditions, with the peat surface 200 mm below the rim (b).

Laboratory tests

Extracted peat samples in both DS and UDS form underwent laboratory testing to evaluate their physicochemical properties, mineral and microstructural characteristics, as well as engineering properties in relation to strength and settlement. These analyses provided insights about the behaviour of peat under various conditions.

Microstructural and mineralogical arrangement

The microstructure of the peat was examined using field emission scanning electron microscopy (FESEM), for which samples were prepared by gold sputtering. This analysis offers magnifications ranging from 500 to 50,000 times, revealing the internal morphology of the peat. Mineralogical composition was determined by energy dispersive X-ray spectroscopy (EDS), which reveals elemental composition as percentages of different elements and gives insights about the nature of soil formation.

Physicochemical and mechanical properties

The physical properties determined were organic content (OC), water content, fibre content (FC), degree of decomposition, soil particle size distribution (sand, silt clay), specific gravity (G), Atterberg (liquid and shrinkage) limits and free swell index (FSI). OC was determined according to the standard ASTM D2974-20 (2020), by igniting samples at 450–500 °C. The standard adopted for water content was IS 2720 (Part 2):1973, and for FC we used ASTM D1997-91 (2013). Decomposition was classified on the von Post scale (H1–H10). Particle size distribution involved H_2O_2 treatment and sedimentation, as per IS 2720 (Part 4):1985. Specific gravity (G) and Atterberg limits (liquid and shrinkage limits) were determined following the guidelines in IS 2720 (Part 3):1980, IS 2720 (Part 5):1985 and IS 2720 (Part 6):1972, while FSI followed IS 2720 (Part 30):1983. Measurements of chemical properties, including pH and cation exchange capacity (CEC), conformed to IS 2720 (Part 24):1976 and IS 2720 (Part 26):1987.

Shear strength was assessed by unconfined compression (UCS), unconsolidated undrained Triaxial (UUTX) and consolidated undrained triaxial (CUTX) tests on elemental samples with a 1:2 aspect ratio, as per IS 2720 (Part 10):1991, IS 2720 (Part 11):1993 and IS 2720 (Part 12):1981. Properties such as cohesion (c), internal friction angle (ϕ), pore water pressure (PWP) and Poisson's ratio (μ) were also evaluated. Settlement properties determined in oedometer tests included compression index (C_c), volume compressibility (m_v) and secondary consolidation (C_α), following IS 2720 (Part 15):1986.

Model-scale tests

Setup for model-scale testing

The model-scale tests were performed to simulate the field environment under controlled laboratory conditions. The setup was designed to replicate in-situ conditions accurately and was consistent with the standardised methodology for model-scale tests provided by Kramer & Stewart (2024). For this purpose, a square steel tank with dimensions 1 m × 1 m × 1 m (length, breadth and height) was utilised. Preparation of the tank involved two distinct phases. In the first phase, the tank was carefully lined with transparent polyethylene sheets to create a watertight barrier and thus prevent any drainage, to ensure that the tests were conducted under strictly undrained conditions. In the second phase, one of the large soil samples collected from the study site was placed in the tank in three layers. Care was taken to distribute each layer evenly across the tank before compacting to in-situ density. The tank was filled to 200 mm below the rim to allow space for the load frame apparatus, as illustrated in Figure 3(b) and Figure 5.

Installation of branched and conventional piles

Piles were prepared using a scaling factor of 1:15, adopted from the studies of Sedran *et al*. (2001), de Sanctis *et al.* (2021) and Vakili *et al.* (2025). Conventionally, piles have a length (L) of 6000 mm and a diameter (D) of 450 mm. For model-scale testing with the specified scaling factor, the piles were designed with L = 400 mm and D = 30 mm, featuring a top frustum cone with maximum diameter 60 mm (= 2D) as illustrated schematically in Figure A1 in the Appendix. The branches were arranged in two whorls ('top' and 'bottom') extending outwards and downwards from the main axis of the pile at various inclination angles (α for top whorl, β for bottom whorl) between 14° and 60°. The branch diameter (D_b) was set at 7 mm. The length of the branches (L_b) was varied in three steps from 1.5D to a maximum of 2.5D (45 mm, 60 mm or 75 mm). The number of branches (n) in each whorl was 2, 3 or 4, and β was always 14° (constrained by the geometry of the frustrum cone). The inclination of the top-whorl branches (α) was systematically adjusted from 14° to 30°, 45° and 60° for successive tests. Detailed schematic diagrams are presented in Figure A1.

The cast-in-situ method was employed to prepare the BPs. A borehole was created in the peat sample using a handheld auger, with formation of the top frustum cone (Figures 4a–d). Then lateral boreholes for the branches were drilled at precise angles, which were measured and maintained using a protractor (Figures 4e–g). The steps in creation of the linked boreholes are also shown as a series of profile sketches in Figure A2 (top). Cement slurry was poured into the borehole to form the pile (Figure 4h). The specification of the cement slurry used is provided in Table A1 in the Appendix. Reinforcements were added, consisting of 3 mm diameter strings (metal wires) for the main pile and 1 mm diameter strings for the branches. The completed structure was left to cure for 28 days to achieve sufficient strength. A top view of the installed BP after setting is shown in Figure 4i.

A conventional pile (CP) without lateral branches was also constructed. In this case, the vertical pile was formed following the same methodology for creation of the main borehole, reinforcement, cement slurry pouring and curing period but omitted the drilling of inclined boreholes to create branch channels. Schematic diagrams comparing structural details of BP and CP can be found in Figure A2.

Loading and settlement tests

To assess the improvement in strength that might be achieved by switching from CP to BP, we carried out loading and settlement analyses (at model scale) involving 36 tests on BP and one test on CP. The experimental setup is shown schematically in Figure 5a, and a photograph is provided in Figure 5b. These Figures illustrate the placement of the piles, hydraulic jack, load cell, dial gauges, and LVDTs, and thus clarify details of the testing setup.

Static loading was applied to the piles using a hydraulic jack mechanism, with applied loads measured precisely by a proving ring of 50 kN capacity. To measure settlement, a hybrid approach incorporating manual and digital techniques was adopted to ensure accuracy and reliability. Dial gauges with an accuracy of 0.01 mm were used alongside two linear variable displacement transducers (LVDTs). The LVDTs were strategically positioned to capture settlement data accurately, accounting for both axial and lateral deformations in the piles. The arrangements for loading and settlement measurements were identical for both BP and CP to ensure consistency in the test conditions.

The CP testing provided a control (baseline) against which any performance enhancement introduced by the branches could be judged. For BP, special attention was paid to exploring the effects of branch geometry, number and inclination angles on load-settlement behaviour.

The data were analysed using the double tangent method (DTM) to evaluate the ultimate bearing capacity (Q_u) of the piles (at failure). Details of the DTM methodology are omitted here for brevity, but may be found by referring to the studies of Borthakur & Dey (2018) and Venkatramaiah (2006).

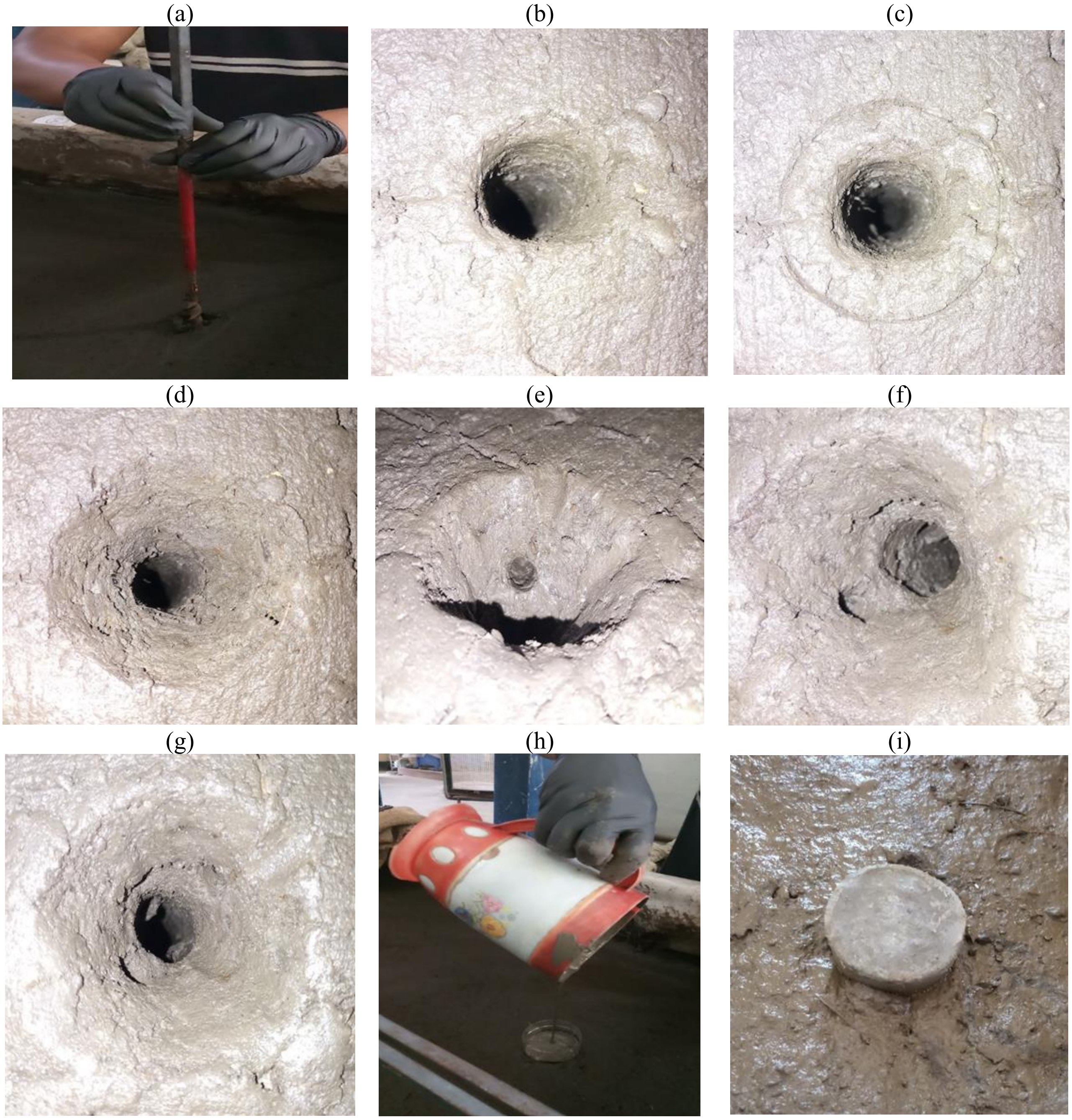

Figure 4. Photographs showing steps in the methodology for installation of branched piles in the model tank. (a) Using a hand auger to drill a vertical hole to the required depth for installation of a pile. (b) A successfully drilled cylindrical borehole, ensuring proper alignment and stability. (c) Adjusting the top of the borehole to shape the conical frustum which provides a platform for test apparatus as well as structural support. (d) The frustum cone was carefully formed, maintaining precise dimensions for uniformity. (e), (f), and (g) illustrate the holes drilled for top and bottom branches, ensuring proper connectivity and alignment. (h) Pouring cement slurry into the prepared borehole to enhance stability and provide structural reinforcement. (i) The BP was successfully installed, completing the setup for further analysis and load application.

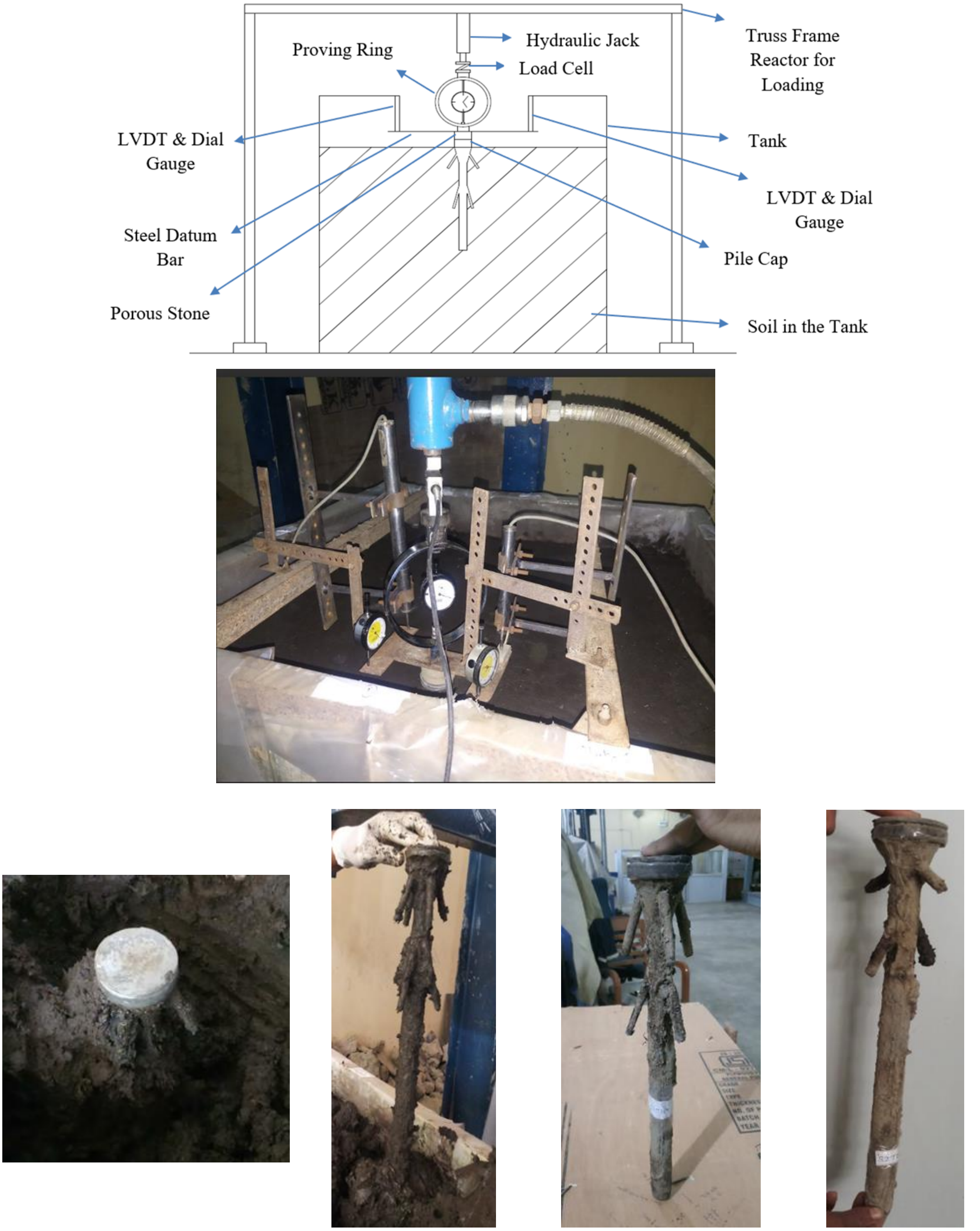

Figure 5. Top: Schematic diagram illustrating a model-scale BP installed in the tank, with labels identifying other components of the experimental setup (hydraulic jack, proving ring, load cell, LVDT). Middle: Photograph of the model-scale tank with key components of the setup in place. Bottom (from left to right): a casted BP in situ and three example BPs extracted from the peat after testing, with 4, 3 and 2 branches per whorl respectively. The extracted piles demonstrate remarkable alignment with the blueprint in terms of structural accuracy and experimental consistency.

RESULTS

In-situ and laboratory tests

The non-invasive ERT and MASW field tests carried out at ETE revealed very low values, with resistivity varying from 16.20 Ω-m to 79.80 Ω-m and V_s ranging from 30.72 m s^{-1} to 120.15 m s^{-1}. A thick deposit of peat was encountered at shallow depth. The vertical profile of the peat layer extended up to 10 m, showing very low SPT-*N* values ranging from 0 to 6 in the penetration tests. The depth of peat changed laterally, varying between a minimum of 6.30 m and a maximum of 10.70 m. Figure 6 presents sample bore logs along with *N* values obtained at different depths. Table 1 provides an overview (average values) of all in-situ test results.

FESEM analysis of oven-dried peat samples (magnifications × 1,000 to × 40,000) revealed fibre entanglement, micro-pores, voids, interstices, clusters, channels, dendrites, stratification, anisotropy and dark patches (Figure 7). The EDS mineralogical classification identified abundant carbon, oxygen and silica accounting for 60 % of the elemental composition, along with trace elements like iron and feldspar. Table 2 summarises the mineralogical composition of the peat.

As far as visual, physicochemical and engineering properties are concerned, the peat was dark brown to blackish in colour with (von Post) degree of humification H7–H8; and FC values ranged from 18.14 % to 24.02 %, which places this deposit in the class sapric peat (FC < 33 %) according to ASTM D1997-91 (2013). OC, which is one of the pivotal peat properties, varied from 52.45 % to 75.02 %. Other crucial physical properties that define peat including water content (w_c), specific gravity of

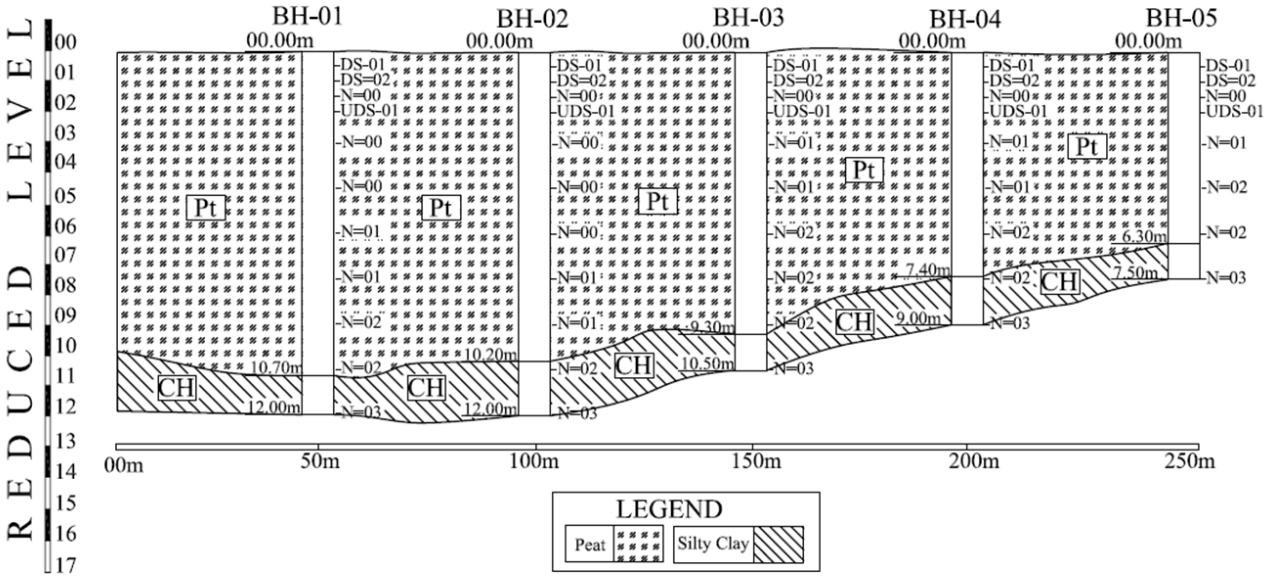

Figure 6. Section through the study site derived from the results of subsoil profiling, showing logged data (SPT-*N* values) from standard penetration tests (SPT). This testing was carried out to highlight variations in composition, density, and stratigraphy of the peat soil across the horizontal extent of the site.

Table 1. Summarised results from the in situ examination of the ETE peat deposit using out non-invasive (ERT, MASW) and invasive (SPT) tests.

Sl.No.	Mode of investigation	Range of results
1.	Electrical resistivity testing, ERT (Ω-m)	8 to 52
2.	Multichannel analysis of surface waves, MASW (m s^{-1})	33.30 to 90.00
3.	Standard penetration test value, N_{60}	0 to 4

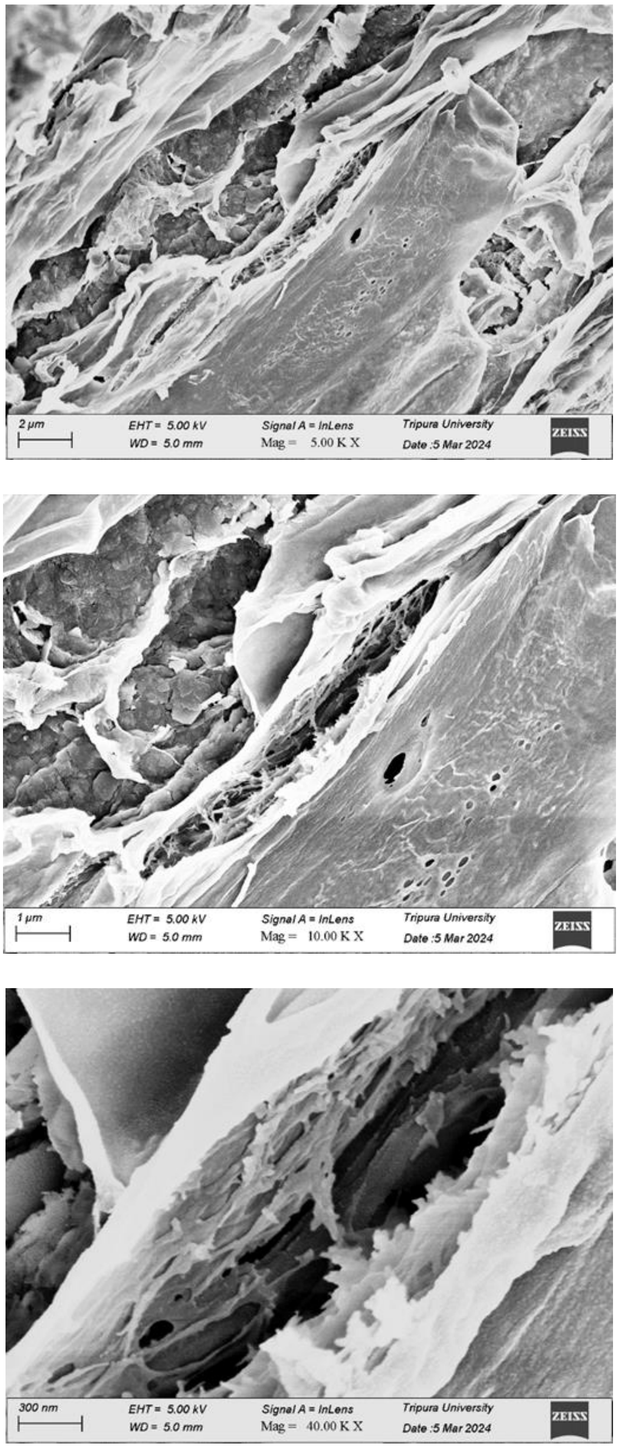

Figure 7. FESEM micrographs of peat samples at magnifications ×5,000 (top), ×10,000 (middle) and ×40,000 times (bottom), showing the highly porous microstructure with excess voids (dark patches) and entangled fibres. These images reveal the intricate arrangement of organic matter with fragmented and degraded cellulose structures, which is reflected in the the weak bonding and high compressibility that is characteristic of peat from the perspective of civil engineering.

particle (G_p), bulk density (γ_b), Atterberg limits (*LL*, *SL*) and FSI are shown in Table 3. The values of chemical properties analysed included pH 4.1–5.4 and CEC 147–509 meq $100g^{-1}$. Such variations are indicative of the differences in composition and geomorphology between different peats, details of which are elaborated in Table 3. From the perspective of strength, the static parameters c and ϕ evaluated from CUTX tests are also presented in Table 3, and ranged from 2 kN m^{-2} to 22 kN m^{-2} and 1° to 8°. A sample graph (c = 0.04 kg cm^{-2}, ϕ = 8° can be found in the Appendix (Figure A3).

Table 2. Mineralogical composition of ETE peat.

Element	% by weight
Oxygen	22.3
Carbon	35.2
Aluminium	12.9
Silica	11.4
Iron	0.7

Table 3. Physicochemical and engineering properties of ETE peat. FC = fibre content, OC = organic content, CEC = cation exchange capacity, w_c = water content, PSA = particle size analysis, G_p = specific gravity of particle, γ_b = bulk density, *LL* = liquid limit, *SL* = shrinkage limit, FSI = free swell index, c = cohesion, ϕ = internal friction angle.

Property	Value
von Post humification	H7–H8
FC (%)	18.14–24.02
Classification based on FC	Sapric (FC < 33 %)
OC (%)	52.45–75.02
pH	4.1–5.4
CEC (meq $100g^{-1}$)	147–509
w_c (%)	719.32–912.04
PSA (%)	S: 01–02 M: 02–04 C: 16–24
G_p	0.613–0.701
γ_b	1.06–1.24
LL (%)	80–99
SL (%)	54–69
FSI (%)	20–30
c (kN m^{-2})	2–22
ϕ (°)	1–8

Settlement curves

The testing to assess the bearing capacity of piles can be divided into two phases. In the first phase, the settlement curves (settlement versus load) of a CP and a BP with the minimum tested values of n, L_b and α were compared. Thus, the specification of the BP was: $n = 2$ (i.e., two branches per whorl), $L_b = 1.5$D (i.e., the branches were 45 mm long) and $\alpha = 14°$ (i.e., all branches were inclined at an angle of 14° to the main axis of the pile). The results are plotted in Figure 8, which shows that BP has a higher load bearing capacity than CP; for example, 189 N versus ~150 N with settlement of 12.50 mm, according to DTM methodology. In the next phase, n, L_b and α were varied as detailed in Methods. The results are shown systematically in Figures 9 and 10.

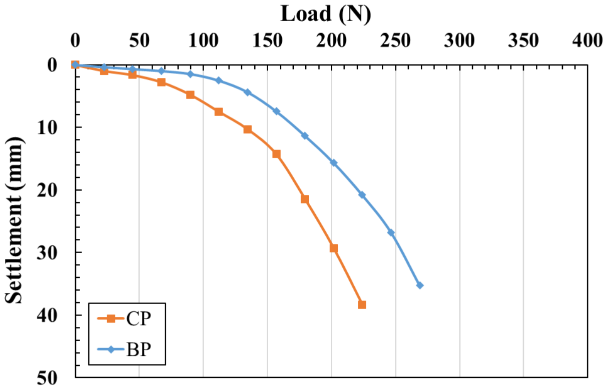

Figure 8. Comparison of the 'baseline' load carrying behaviour of CP (without branches) and BP with the lowest tested values of n, L_b and α; i.e., two 45-mm branches per whorl, all inclined at 14° to vertical.

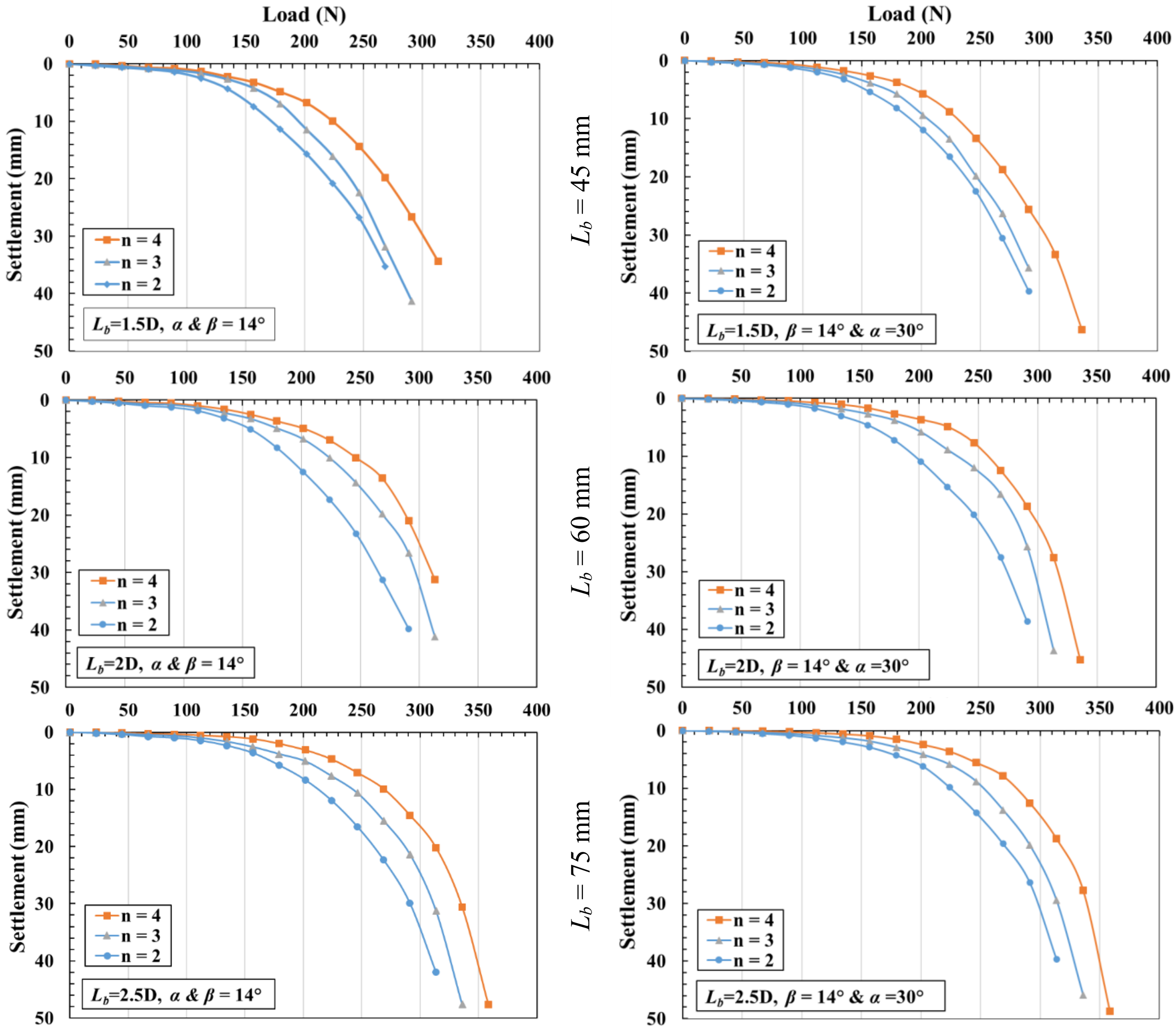

Figure 9. Graphs comparing the load carrying behaviour of BP with different numbers of branches (n) per whorl and different lengths (L_b), with top branch inclination (α) 14° (left) or 30° (right).

All panels in Figures 9 and 10 show clearly that the load-carrying capacity increased as the number of branches per whorl was increased from 2, through 3 to 4. Comparing between rows from top to bottom of each column shows that increasing the length of branches L_b from 1.5D through 2D to 2.5D further enhanced the load-carrying capacity. Finally, comparing between columns from left to right across the two Figures shows that increasing the inclination of top branches (α) from 14°, through 30° to 45° also increased capacity, although this trend did not continue strongly at α = 60°. Values of Q_u for all of the tests carried out are shown in in Table 4.

Variation of load capacity of piles with n, L_b and α

As demonstrated by the compression test results, the design specifications for n, L_b, and α significantly influenced load-carrying capacity and settlement of BP. To comprehensively evaluate these effects we adopted an analytical approach utilising an Improvement Factor (IF), defined as:

$$IF = \frac{Q_u \; of \; BP - Q_u \; of \; CP}{Q_u \; of \; CP} \qquad [1]$$

where Q_u is the ultimate bearing capacity of BP or CP. The IF serves as a quantitative measure to assess the

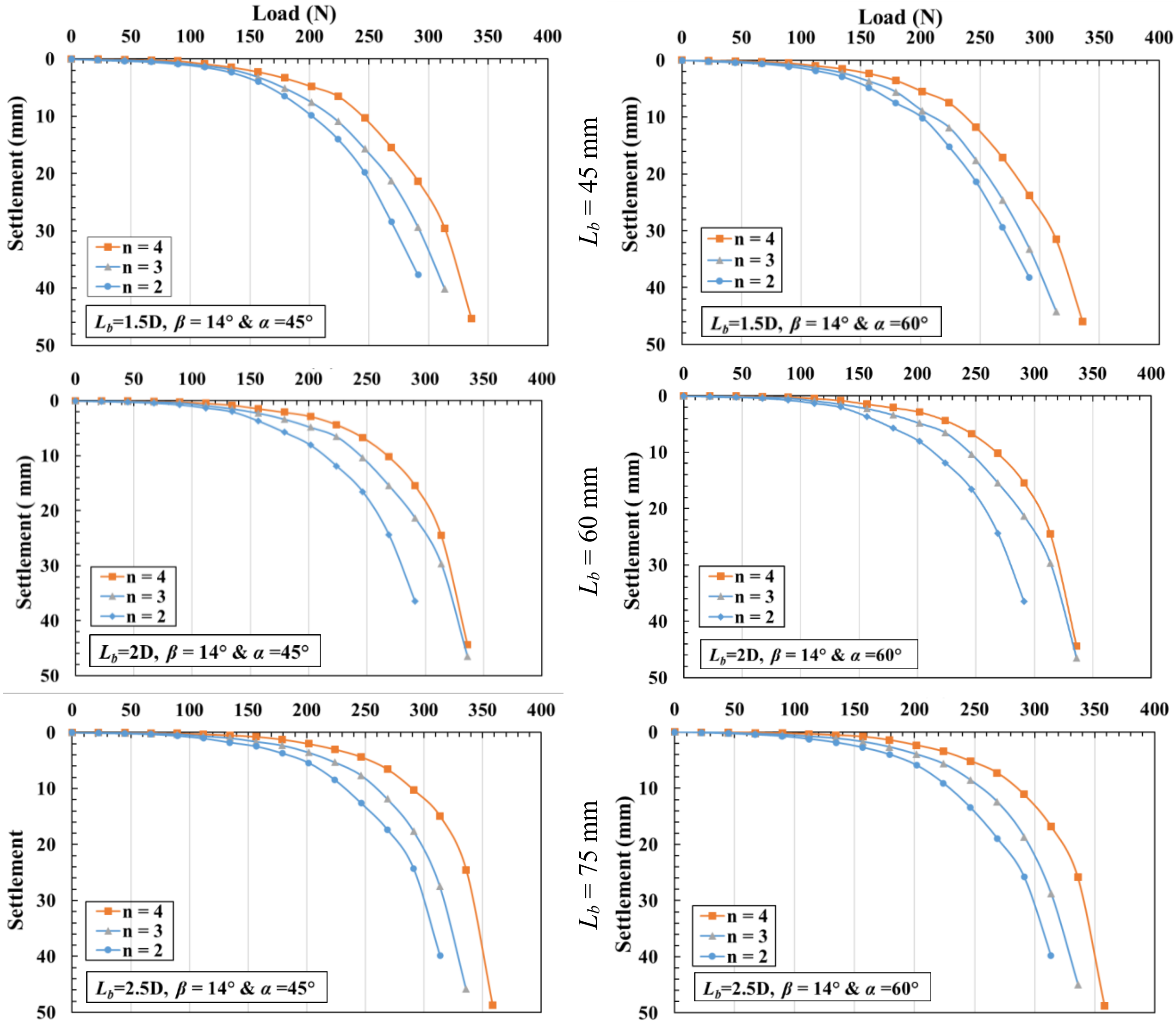

Figure 10. Graphs comparing the load carrying behaviour of BP with different numbers of branches (n) per whorl and different lengths (L_b), with top branch inclination (α) 45° (left) or 60° (right).

combined influence of n, L_b and α on the overall performance of the piles under different conditions. A detailed analysis was conducted to explore the relationship between IF and the factors n, L_b and α, shown graphically in Figures A4 to A6. The *IF* values ranged from 0.20 to 1.40, with lower values corresponding to configurations with reduced load-carrying capacity and less favourable settlement performance and higher *IF* values linked to enhanced pile performance, reflecting optimal combinations of the design factors. For effective pile design and performance optimisation, the critically important step involves carefully selecting and varying n, L_b and α to achieve the desired load-carrying capacity while minimising settlement.

DISCUSSION

This study has introduced the BP methodology as an effective solution for enhancing strength and reducing settlement of constructions on peat. It bridges the gap between researchers and engineers, offering a practical approach that combines theoretical insights with field implementation. The BP methodology addresses common peat stabilisation challenges, providing sustainable, cost-effective ground improvement solutions while encouraging further advancements in geotechnical engineering. The combination of field and laboratory analyses undertaken has also provided critical insights about geotechnical properties of the soil.

Table 4. Bearing capacity of peat obtained using the double tangent method (DTM). CP: conventional pile; *BP*: branched pile; n: number of branches per whorl (top and bottom); L_b: length of branches; α: inclination angle of top-whorl branches; Q_u: ultimate bearing capacity; IF: Improvement Factor (Equation 1) expressed as a percentage.

Pile type	n	L_b		$\alpha = 14^o$		$\alpha = 30^o$		$\alpha = 45^o$		$\alpha = 60^o$	
		(formula)	(mm)	Q_u (N)	IF (%)	Q_u (N)	IF (%)	Q_u (N)	IF (%)	Q_u (N)	IF (%)
CP	0	0	n/a	143							
BP	2	1.5D	45	189	32	200	40	207	45	203	42
		2D	60	198	38	220	54	230	61	225	57
		2.5D	75	239	67	254	78	265	85	259	81
	3	1.5D	45	203	42	223	56	234	64	228	59
		2D	60	252	76	265	85	275	92	269	88
		2.5D	75	271	90	280	96	290	103	284	99
	4	1.5D	45	254	78	264	85	280	96	272	90
		2D	60	274	92	286	100	295	106	281	97
		2.5D	75	300	110	314	120	323	126	318	122

The model-scale tests are critical. Replicating field conditions on a smaller scale has allowed a detailed examination of peat behaviour under simulated loading, deformation and environmental conditions providing valuable data to complement the findings from elemental and laboratory analyses.

Field and laboratory geotechnical experiments

Geophysical and geotechnical investigations of peat carried out at eight different locations within the ETE site revealed significant variations in nature of the (sapric) peat, for example in its OC (55–79 %). ERT results ranged from 16.20 Ω-m to 79.80 Ω-m, which are very low values influenced by peat properties such as high OC, decomposition, low FC, high moisture retention, presence of conductive minerals, pore fluid salinity, fine-grained soil fraction, degree of humification and leaching of dissolved ions. Similarly low resistivity values (15–90 Ω-m) were recorded in the studies of Basri *et al.* (2019), Debnath *et al.* 2021, Nurmaisarah *et al.* (2023) and Hasan *et al.* (2025). The ERT tests were complemented by MASW surveys which recorded very low values of V_s (30.72–120.15 m s^{-1}), reflecting factors such as high water content, organic matter, low density, high void ratio, weak interparticle bonding, low stiffness of the soil matrix, high compressibility, loose particle packing and the presence of gas bubbles or biogenic materials. The studies of Lee & Youventaran (2022), Zainorabidin *et al.* (2023), Kibria (2024) and Hasan *et al.* (2025) have also reported low V_s values whose range (13.80–100.00 m s^{-1}) falls well within the range of values observed in the present study. The invasive geotechnical testing (SPT) also indicated very soft soil with very low N_{60} values with range 0–3, primarily owing to high organic matter, low density, spongy and humous nature, high moisture content, high void ratio, weak soil structure, compressibility, low shear strength and the presence of fibrous or decomposed peat fragments. Our SPT values are in good agreement with those stated by Wang *et al.* (2023), Al-Ani *et al.* (2013), Das *et al.* (2023) and Debnath *et al.* (2024). The microstructural analysis highlighted porous fabrics, twisted fibres and decomposed remains, corroborating high void ratio, water retention and weak interparticle bonding. The presence of dark patches in the micrographs provides deep insights into the presence of zones of enhanced decomposition, accumulation of organic residues and potential areas of mineral deposition, further emphasising the heterogeneity and complex structure of the soil matrix. The intricate morphology of ETE peat aligns well with the findings of Paul *et al.* (2021), Debnath *et al.* (2021), de Araujo *et al.* (2023), Ahmad *et al.* (2024) and Wilson (2025). Mineralogical analysis confirmed the presence of significant amounts of oxygen and carbon amounting to more than 50 % of total elemental composition, which is well supported by the research findings of Gao *et al.* (2019), Paul *et al.* (2021), Wen *et al.* (2020) and Cao *et al.* (2022). Our observations of physicochemical properties such as high water content (710.02–918.65 %), specific gravity (0.599–0.715), organic content (50.05–79.02 %), clay content (14–49 %) and acidic pH (3.6–5.1) aligned well with established characteristics of tropical peat. CEC values (147.2–509.2 meq 100cm^{-3}) indicated strong ion exchange potential. Bulk density values were 10.21–14.65 kN m^{-3}, and Atterberg tests showed high liquid limits. Such abnormalities in the physical properties of peat (as a soil) are attributed primarily to its prolonged waterlogging, anaerobic decomposition, high organic accumulation, elevated porosity, fibrous structure and humification (Johari *et al.* (2016), Phang *et al.* (2022), Debnath *et al.* (2024), Novrianti & Harisuseno (2024), Muhammad & Jethoo (2025).

Low shear strength parameters (c = 3–12 kN m^{-2}, ϕ = 4–12°) indicate very soft to soft soil arising from its porous nature, low density and high OC. High PWP development is attributed to entrapped water. Our values of effective stress align with those of Kazemain *et al.* (2012), Paul & Hussain (2019) and Zimar *et al.* (2020). Settlement parameters (C_c = 2.01–3.72) resemble values from Islam & Hashim (2010), Ulusay *et al.* (2010) and Zimar *et al.* (2020) while other settlement parameters (a_v, m_v, C_v) match those from Ulusay *et al.* (2010) and Amuda *et al.* (2019). Compression ratio (0.37–0.50) agrees with Hebib & Farrell (2003), Debnath *et al.* (2022) and Zainorabidin *et al.* (2024), exceeding 0.20 (O'Loughlin & Lehane 2003) and confirming high compressibility.

Load-settlement response curves

The load-settlement response curves in Figure 8 clearly demonstrate that BP offers a significant improvement in Q_u calculated using the DTM approach. For instance, Q_u for BP (with $n = 2$, $L_b = 1.5$ D, $\alpha = 14°$) is increased by 32 % compared to CP. The trend of improvement continues consistently as number and length of branches and branch angle are increased, to a maximum IF value of 126 % (with $n = 4$, $L_b = 2.5$ D, $\alpha = 45°$). The performance enhancements (overall increase in bearing capacity) can be attributed to the multiple branches providing a larger load transfer area and increased lateral soil resistance, as in the studies of Dash & Bora (2013) and Shahrour & Rezaie (1997). However, it should be noted that Q_u shows a declining trend when the α

value exceeds 45°. This behavior can be linked to the loss of optimal soil confinement around the branches, leading to stress concentration and premature failure (Poulos & Davis 1980). At excessively high branch angles, the load transfer efficiency reduces due to increased local shear failure and reduced effective interlocking between the pile and the surrounding soil (Meyerhof 1976, Knellwolf *et al.* 2011). Thus, it can be concluded from the results observed that branching enhances pile performance but there is an optimal configuration beyond which structural inefficiencies emerge. Similar findings have been reported from experimental and numerical studies of bio-inspired pile geometries and expanded base foundations (Nguyen & Likitlersuang 2019, Giretti *et al.* 2022). Recent studies further corroborate these observations, emphasising the importance of optimising pile configuration to balance performance and structural integrity (Smith *et al.* 2023, Lee *et al*. 2024, Zhang *et al.* 2025, Patel & Singh 2025).

Influence of branch count on the load-bearing performance of branched piles

To evaluate the influence of n on Q_u (derived using the DTM method), tests with varying n (range 2–4) and constant values for L_b and α were considered. For a branch length of 1.5D and α = 14°, increasing n from 2 to 4 resulted in a significant (~50 %) improvement in Q_u from 189 N to 254 N, increasing the IF from 32 % to 78 % (Table 4, Figure A4). The increase in Q_u with higher branch count can be attributed to the improved stress distribution, greater lateral resistance and increased shaft–pile interaction, as found in several previous studies (Goh *et al.* 2018, Zhang *et al.* 2023, Goh & Yann 2021, Chen *et al.* 2022, Wang *et al.* 2023, Singh *et al.* 2024, Patel *et al.* 2025, Huang *et al.* 2025). The enhancement in bearing capacity also aligns with the findings of Meyerhof (1976), who emphasised the contribution of pile geometry to load-bearing performance. The results are also consistent with the work of Poulos (1987), which highlighted the role of pile modifications in augmenting axial load resistance. These findings indicate that load-bearing capacity can be optimised by strategically incorporating additional branches, making BP an effective alternative to CP in geotechnical applications.

Influence of branch length and inclination angle on bearing capacity of piles

To gain insights about the combined influence of L_b and α on Q_u, we considered the changes shown in Table 4 for scenarios where L_b was varied from 1.5D to 2.5D (see Figure A4) and α from 14° to 60°, while keeping n constant. For the case with two branches per whorl ($n = 2$), Q_u increased significantly from 189 N to 265 N (by ~36 %) and the IF was raised from 32 % to 81 %, when L_b and α were changed from their minimum to their maximum values. Increased Q_u with larger L_b and α can be attributed to improved load distribution, increased shaft resistance and enhanced stress transfer as found in previous studies (Chen *et al.* 2022, Wang *et al.* 2023, Singh *et al.* 2024, Patel *et al.* 2025, Huang *et al.* 2025). These findings again align with Meyerhof (1976), who emphasised the importance of pile geometry in optimising bearing capacity. Poulos & Davis (1980) further established that varying pile modifications could significantly enhance axial load resistance. Thus, optimising L_b and α in BP design can substantially improve load-bearing performance, making BP an efficient alternative to CP in various geotechnical applications (Goh & Yann 2021). However, the detailed results also revealed that Q_u actually decreased by 6N when the α value was increased beyond 45°. Hence, our data infer that maximum bearing capacity is achieved when $\alpha = 45°$ (see also Figure A5).

Influence of branch count, length and angle on branched piles

The combined effect of n, L_b and α on Q_u can also be assessed using Table 4. When L_b was changed from 1.5D to 2.5D, α from 14° to 45° (optimum inclination, see above) and n were from 2 to 4, Q_u increased by 70 %, from 189 N to 323 N, and the IF from 32 % to 126 %. The combined effect of increasing n, L_b and α results in increased load-carrying capacity due to synergistic reinforcement of the soil–pile interaction. Higher n facilitates better force redistribution, minimising stress concentrations and enhancing stability. Greater L_b and optimal α ($\leq 45°$) create a more extensive failure surface, improving overall pile performance. Lastly, energy dissipation capacity is enhanced, reducing the risk of failure under cyclic and dynamic loads. These findings confirm the role of branch configurations in improving pile performance under varying load conditions (Chen *et al.* 2022, Wang *et al.* 2023). The greater soil–pile interaction originating from a higher n introduces additional bearing surfaces, increasing shaft resistance and efficiency by improving resistance to stress, enhanced lateral stiffness, increased end-bearing efficiency and reduced long-term settlement (Singh *et al.* 2024, Patel *et al.* 2025, Huang *et al.* 2025). Increased passive resistance mobilises additional earth pressure, enhancing lateral and vertical resistance (Meyerhof 1976, Poulos & Davis 1980). Optimised pile geometry with larger L_b and α reduces load-induced deformation, improving serviceability (Goh & Yann 2021). These findings confirm the role of branch configuration in improving pile performance under varying loading conditions.

Based on the discussion above, there seems to be a relationship between the geotechnical and geophysical behaviour of sapric tropical peat and the efficiency of Branched Pile (BP) systems. Our field and laboratory results reveal the high organic content, compressibility and weak structure of peat which jointly underlie its poor engineering performance. However, load–settlement analysis based on the Double Tangent Method (DTM) demonstrates that the performance (in terms of bearing capacity) of foundations on these weak organic deposits can be improved by up to 122 % using BP configurations with branch count, length and inclination adjusted for optimal load transfer and lateral resistance.

ACKNOWLEDGEMENTS

The authors acknowledge the laboratory personnel (Soumitra Kumar Kundu, Faizal Haque Choudhury, Biswajit Debnath) and the facilities provided by the Centre for Testing and Consultancy, Department of Civil Engineering, NIT Silchar.

AUTHOR CONTRIBUTIONS

DKJ conceptualised the stabilisation technique, conducted the field and laboratory investigations, wrote the original version of the manuscript, prepared the layout of the article, and edited and reviewed the manuscript, Figures and Tables. AKD conceptualised the stabilisation technique and reviewed the manuscript, Figures and Tables. RD undertook the field investigation plus writing, editing and reviewing of the manuscript and Figures.

REFERENCES

Ahmad, A., Karunatilaka, D.S., Anggraini, V., Raghunandan, M.E. (2024) Mechanical, micro-structural, and environmental performance of industrial byproducts in peat reinforcement. *Construction and Building Materials*, 451, 138780. https://doi.org/10.1016/j.conbuildmat.2024.138780

Akhtar, H., Lupascu, M., Sukri, R.S. (2022) Interactions between microtopography, root exudate analogues and temperature determine CO_2 and CH_4 production rates in fire-degraded tropical peat. *Soil Biology and Biochemistry*, 169, 108646. https://doi.org/10.1016/j.soilbio.2022.108646

Al-Ani, H., Oh, E., Chai, G. (2013) Engineering properties of peat in estuarine environment. In: *Foundation and Soft Ground Engineering Conference Thu Dau Mot University ICTDMU-1, Binh Duong, June 5–6*, University of Thu Dau Mot & Construction Publishing House, 181–192. https://research-repository.griffith.edu.au/server/api/core/bitstreams/15cd3a07-9f9c-5225-aa52-06c57670cda1/content

Amuda, A.G., Hasan, A., Unoi, D.N.D., Taib, S.N.L. (2019) Strength and compressibility characteristics of amorphous tropical peat. *Journal of GeoEngineering*, 14(2), 85–96.

Anuar, N.H.H.M., Hasbollah, D.Z.A., Zukri, A. (2024) Stabilizing peat soil using sawdust ash. *Smart and Green Materials*, 1(1), 1–12. https://doi.org/10.70028/sgm.v1i1.2

ASTM D1997-91 (2013) Standard Test Method for Laboratory Determination of the Fiber Content of Peat Samples by Dry Mass. ASTM International, West Conshohocken, PA, USA.

ASTM D2974-20 (2020) Standard Test Methods for Determining the Water (Moisture) Content, Ash Content, and Organic Material of Peat and Other Organic Soils. ASTM International, West Conshohocken, Pennsylvania, USA.

Bakhir, M.A., Talib, M.A., Madun, A., Dan, M.M., Pakir, F., Yusof, Z.M. (2024) Stabilization of peat using sugarcane bagasse ash (SCBA) and cement as a stabilizer. *IOP Conference Series: Earth and Environmental Science*, 1347, 012078. https://doi.org/10.1088/1755-1315/1347/1/012078

Basri, K., Wahab, N., Talib, M.K.A., Zainorabidin, A. (2019) Sub-surface profiling using electrical resistivity tomography (ERT) with complement from peat sampler. *Civil Engineering and Architecture*, 7(6A), 7–18. https://doi.org/10.13189/cea.2019.071402

Borthakur, N., Dey, A.K., (2018) Experimental investigation on load carrying capacity of micropiles in soft clay. *Arabian Journal for Science and Engineering*, 43(4), 1969–1981. https://doi.org/10.1007/s13369-017-2894-3

Cao, C., Huang, J., Ge, L., Li, T., Bu, Z.J., Wang, S., Wang, Z., Liu, Z., Liu, S., Wang, M. (2022) Does shift in vegetation abundance after nitrogen and phosphorus additions play a key role in regulating fungal community structure in a northern peatland? *Frontiers in Microbiology*, 13, 920382. https://doi.org/10.3389/fmicb.2022.920382

Chen, L., Chong, J., Pang, L., Zhang, C. (2022) Lateral capacity of a two-pile group foundation model located near slope in sand. *Ocean Engineering*, 266, 112847.

https://doi.org/10.1016/j.oceaneng.2022.112847

Das, N., Darshan, B., Nanthagopalan, P. (2023) Ballistic impact: predicting penetration depth in ultra-high-performance concrete targets. *Proceedings of the Institution of Civil Engineers - Construction Materials*, 177(4), 215–232. https://doi.org/10.1680/jcoma.23.00006

Dash, S.K., Bora, M.C. (2013) Influence of geosynthetic encasement on the performance of stone columns floating in soft clay. *Canadian Geotechnical Journal*, 50(7), 754–765. https://doi.org/10.1139/cgj-2012-0437

de Araújo, K.V., Horák-Terra, I., da Silva Terra, F., Dobbss, L.B. (2023) Anthropic interventions change the soil properties of savanna palm swamps (veredas) from Central Brazil. *Geoderma Regional*, 33, e00644. https://doi.org/10.1016/j.geodrs.2023.e00644

de Sanctis, L., Di Laora, R., Garala, T.K., Madabhushi, S.P.G., Viggiani, G.M.B., Fargnoli, P. (2021) Centrifuge modelling of the behaviour of pile groups under vertical eccentric load. *Soils and Foundations*, 61(2), 465–479. https://doi.org/10.1016/j.sandf.2021.01.006

Debnath, R., Saha, R., Haldar, S. (2021) Static and dynamic characterisation of Agartala peat. *Mires and Peat*, 27, 25. https://doi.org/10.19189/MaP.2020.BG.StA.2132

Debnath, R., Saha, R., Haldar, S. (2022) Assessment of small strain dynamic soil properties of railway site Agartala, India, by bender element tests. *Arabian Journal of Geosciences*, 15(18), 1500. https://doi.org/10.1007/s12517-022-10749-4

Debnath, R., Das, R., Kumar, R., Saha, R. (2024) Seismic hazard assessment of Agartala agglomeration based on 1D nonlinear ground response analysis and empirically derived liquefaction susceptibility. *Acta Geophysica*, 73, 2181–2215. https://doi.org/10.1007/s11600-024-01502-4

Gao, C., Zhang, S., Li, Y., Han, D., Liu, H., Wang, G. (2019) Holocene mercury accumulation calibrated by peat decomposition in a peat sequence from the Sanjiang Plain, northeast China. *Quaternary International*, 527, 19–28. https://doi.org/10.1016/j.quaint.2019.01.020

Giretti, D., Fioravante, V., Perini, L., Calabrese, L. (2022) Consolidation settlement of coastal areas of the Emilia-Romagna region from cone penetration tests. In: Gottardi, G., Tonni, L. (eds.) *Cone Penetration Testing 2022*, Proceedings of the 5th International Symposium on Cone Penetration Testing (CPT'22), 8–20 June 2022, Bologna, Italy, CRC Press, London UK, 949–954. https://doi.org/10.1201/9781003308829-142

Goh, A.M., Yann, X.L. (2021) Food-image classification using neural network model. *International Journal of Electronics Engineering and Applications*, 9(3), 12–22. https://doi.org/10.30696/IJEEA.IX.III.2021.12-22

Goh, P.S., Lau, W.J., Othman, M.H.D., Ismail, A.F. (2018) Membrane fouling in desalination and its mitigation strategies. *Desalination*, 425, 130–155. https://doi.org/10.1016/j.desal.2017.10.018

Hasan, M.M., Rahman, M.Z., Fahim, A.K.F. (2025) Earthquake induced liquefaction hazard analysis for Chittagong City using machine learning. *Geomatics, Natural Hazards and Risk*, 16(1), 2451126. https://doi.org/10.1080/19475705.2025.2451126

Hassan, N.S.I.A., Hasbollah, D.Z.A., Muztaza, N.M., Yuliana, Y. (2024) Peat soil stabilizer using plastic waste. *Smart and Green Materials*, 1(1), 44–56. https://doi.org/10.70028/sgm.v1i1.4

Hebib, S., Farrell, E.R. (2003) Some experiences on the stabilization of Irish peats. *Canadian Geotechnical Journal*, 40(1), 107–120. https://doi.org/10.1139/t02-091

Huang, Q., Wu, Y., Huang, S., Chen, G., Zhang, S., Zhang, F. (2025) Numerical tests on dynamic response of embankment with pile-supported foundation for high-speed railway in soft ground using soil–water coupling elastoplastic FEM. *Scientific Reports*, 15, 5651. https://doi.org/10.1038/s41598-025-89619-4

IS 2131:1981 - Method for Standard Penetration Test for Soils, Bureau of Indian Standards, New Delhi, India.

IS 2720 (Part 2):1973 - Methods of Test for Soils: Part 2 Determination of Water Content. Bureau of Indian Standards, New Delhi, India.

IS 2720 (Part 3):1980 - Methods of Test for Soils: Part 3 Determination of Specific Gravity. Bureau of Indian Standards, New Delhi, India.

IS 2720 (Part 4):1985 - Methods of Test for Soils: Part 4 Grain Size Analysis. Bureau of Indian Standards, New Delhi, India.

IS 2720 (Part 5):1985 - Methods of Test for Soils: Part 5 Determination of Liquid and Plastic Limit. Bureau of Indian Standards, New Delhi, India.

IS 2720 (Part 6):1972 - Methods of Test for Soils: Part 6 Determination of Shrinkage Factors. Bureau of Indian Standards, New Delhi, India.

IS 2720 (Part 10):1991 - Methods of Test for Soils: Part 10 Determination of Unconfined Compressive Strength. Bureau of Indian Standards, New Delhi, India.

IS 2720 (Part 11):1993 - Methods of Test for Soils: Part 11 Determination of Shear Strength Parameters Using Direct Shear Test. Bureau of

Indian Standards, New Delhi, India.

IS 2720 (Part 12):1981 - Methods of Test for Soils: Part 12 Determination of Shear Strength Parameters of Saturated Soils Using Triaxial Compression Test. Bureau of Indian Standards, New Delhi, India.

IS 2720 (Part 15):1986 - Methods of Test for Soils: Part 15 Determination of Consolidation Properties. Bureau of Indian Standards, New Delhi, India.

IS 2720 (Part 24):1976 - Methods of Test for Soils: Part 24 Determination of Cation Exchange Capacity. Bureau of Indian Standards, New Delhi, India.

IS 2720 (Part 26):1987 - Methods of Test for Soils: Part 26 Determination of pH. Bureau of Indian Standards, New Delhi, India.

IS 2720 (Part 30):1983 - Methods of Test for Soils: Part 30 Determination of Free Swell Index of Soils. Bureau of Indian Standards, New Delhi, India.

Islam, M.S., Hashim, R., (2010) Behaviour of stabilised peat: A field study. *Scientific Research and Essays*, 5, 2366–2374.

Johari, N.N., Bakar, I., Razali, S.N.M., Wahab, N. (2016) Fiber effects on compressibility of peat. *IOP Conference Series: Materials Science and Engineering*, 136, 012036. https://doi.org/10.1088/1757-899X/136/1/012036

Jorat, M.E., Minto, A., Tierney, I., Gilmour, D. (2024) Future carbon-neutral societies: minimising construction impact on groundwater-dependent wetlands and peatlands. *Sustainability*, 16(17), 7713. https://doi.org/10.3390/su16177713

Kazemian, S., Huat, B.B., Moayedi, H. (2012) Undrained shear characteristics of tropical peat reinforced with cement stabilized soil column. *Geotechnical and Geological Engineering*, 30, 753–759. https://doi.org/10.1007/s10706-012-9492-7

Khanday, S.A., Ahongshangbam, D., Hussain, M. (2022) Durability of peat stabilized with RHA-based geopolymer formed by adding pure alumina. *International Journal of Geosynthetics and Ground Engineering*, 8(5), 54. https://doi.org/10.1007/s40891-022-00399-7

Kibria, S. (2024) *Using ERI and MASW to Assess Highway Slopes and Levees*. Master's thesis, Jackson State University, Jackson MS, 114 pp.

Knellwolf, C., Peron, H., Laloui, L. (2011) Geotechnical analysis of heat exchanger piles. *Journal of Geotechnical and Geoenvironmental Engineering*, 137(10), 890–902. https://doi.org/10.1061/(ASCE)GT.1943-5606.0000513

Kramer, S.L., Stewart, J.P. (2024) *Geotechnical Earthquake Engineering*. CRC Press, Boca Raton, 1060 pp.

Kundu, S.K., Saha, A., Dey, A.K., (2024. Electrical resistivity tomography to check compaction control of road embankment made of partially saturated soil. *Innovative Infrastructure Solutions*, 9(7), 283. https://doi.org/10.1007/s41062-024-01605-3

Lee, K., Youventharan, D. (2022) Shear wave velocity measurements in tropical peat using in-house device. *Construction*, 2(1), 22–30. https://doi.org/10.15282/construction.v2i1.7404

Lee, K., Kim, M., Hwang, T. (2024) Reinforcement effect of micropile and bearing characteristics of micropiled raft according to the cohesion of soil and stiffness of pile. *Geomechanics & Engineering*, 37(5), 511–525.

Li, N., Li, M., Sack, D., Kang, W., Song, L., Yang, Y., Zong, Y., Jie, D. (2020) Diatom evidence for mid-Holocene peatland water-table variations and their possible link to solar forcing. *Science of the Total Environment*, 725, 138272. https://doi.org/10.1016/j.scitotenv.2020.138272

Meyerhof, G.G. (1976) Bearing capacity and settlement of pile foundations. *Journal of the Geotechnical Engineering Division*, 102(3), 197–228. https://doi.org/10.1061/AJGEB6.0000243

Muhammad, S.A., Jethoo, A.S. (2025) Harnessing microbial-induced calcite precipitation for sustainable seepage control in cohesionless soil channels. *Geomicrobiology Journal*, 42(2), 147–163. https://doi.org/10.1080/01490451.2024.2439919

Nguyen, T.S., Likitlersuang, S. (2019) Reliability analysis of unsaturated soil slope stability under infiltration considering hydraulic and shear strength parameters. *Bulletin of Engineering Geology and the Environment*, 78, 5727–5743. https://doi.org/10.1007/s10064-019-01513-2

Novrianti, Harisuseno, D. (2024) Correlation between volume weight, porosity and moisture content in Central Kalimantan's Peatlands. *IOP Conference Series: Earth and Environmental Science*, 1311, 012047. https://doi.org/10.1088/1755-1315/1311/1/012047

Nurmaisarah, Z.S., Baba, M., Mohamad, H.M., Hardianshah, S. (2023) Geoelectrical characterization of the peat soil at Klias Peninsula, Beaufort, Sabah (Malaysia). *Iranian Journal of Geophysics*, 17(3), 27–44.

O'Loughlin, C., Lehane, B. (2003) A study of the link between composition and compressibility of peat and organic soils. In: Huat, B.B.K., Omar, H., Maail, S., Mahsun, E. (eds.) *Proceedings of the 2nd Conference on Advances in Soft Soil Engineering and Technology*, Universiti Putra Malaysia Press, Serdang, Selangor MY, 135–152.

Patel, M., Singh, B. (2025) Evaluation of the impacts of phased excavation of shield tunnel on adjacent piled raft foundation of a building. In: Satyam, N., Singh, A.P., Dixit, M.S. (eds.) *Proceedings of 91YGEC 2023, Volume 2* (Indian Young Geotechnical Engineers Conference IYGEC 2021), Lecture Notes in Civil Engineering 606, Springer, Singapore, 183–196. https://doi.org/10.1007/978-981-97-6988-9_19

Patel, M., Chaudhary, V., Verma, V., Kumar, A., Kakati, B.K. (2025) Advances in ground heat exchangers and thermal energy storage for sustainable energy systems. *Indian Chemical Engineer*, 67(4), 429–449. https://doi.org/10.1080/00194506.2025.2454246

Paul, A., Hussain, M. (2019) Geotechnical properties and microstructural characteristics of Northeast Indian peats. *Mires and Peat*, 24, 07. https://doi.org/10.19189/MAP.2018.BG.376

Paul, A., Hussain, M. (2020) Cement stabilization of Indian peat: an experimental investigation. *Journal of Materials in Civil Engineering*, 32(11), 04020350. https://doi.org/10.19189/MAP.2018.BG.376

Paul, A., Hussain, M., Ramu, B. (2021) The physicochemical properties and microstructural characteristics of peat and their correlations: reappraisal. *International Journal of Geotechnical Engineering*, 15(6), 692–703. https://doi.org/10.1080/19386362.2018.1483099

Phang, I.R.K., Wong, K.S., Chan, Y.S., Lau, S.Y. (2022) Effect of microbial-induced calcite precipitation towards strength and permeability of peat. *Bulletin of Engineering Geology and the Environment*, 81(8), 314. https://doi.org/10.1007/s10064-022-02790-0

Poulos, H.G. (1987) Analysis of residual stress effects in piles. *Journal of Geotechnical Engineering*, 113(3), 216–229. https://doi.org/10.1061/(ASCE)0733-9410(1987)113:3(216)

Poulos, H.G., Davis, E.H. (1980) *Pile Foundation Analysis and Design*. First edition, John Wiley & Sons Limited, Chichester UK, 307 pp. ISBN: 0-471-02084-2.

Raut, Z.P., Verma, M.P. (2024) Comprehensive review of soil stabilization through reinforcement methods in civil engineering. *International Journal of Innovative Research in Technology and Science*, 12(2), 520–530. https://doi.org/10.22214/ijraset.2024.65827

Sabrekov, A.F., Terentieva, I.E., McDermid, G.J., Litti, Y.V., Prokushkin, A.S., Glagolev, M.V., Petrozhitskiy, A.V., Kalinkin, P.N., Kuleshov, D.V., Parkhomchuk, E.V. (2023) Methane in West Siberia terrestrial seeps: Origin, transport, and metabolic pathways of production. *Global Change Biology*, 29(18), 5334–5351. https://doi.org/10.1111/gcb.16863

Saha, A., Nath, A., Dey, A.K. (2022) Multivariate geophysical index-based prediction of the compression index of fine-grained soil through nonlinear regression. *Journal of Applied Geophysics*, 204, 104706. https://doi.org/10.1016/j.jappgeo.2022.104706

Sarangi, V., Roy, S., Sanyal, P. (2022) Effect of burning on the distribution pattern and isotopic composition of plant biomolecules: Implications for paleoecological studies. *Geochimica et Cosmochimica Acta*, 318, 305–327. https://doi.org/10.1016/j.gca.2021.12.003

Schneider, E., Rüger, C.P., Chacón-Patiño, M.L., Somero, M., Ruppel, M.M., Ihalainen, M., Köster, K., Sippula, O., Czech, H., Zimmermann, R. (2024) The complex composition of organic aerosols emitted during burning varies between Arctic and boreal peat. *Communications Earth & Environment*, 5(1), 137. https://doi.org/10.1038/s43247-024-01304-y

Sedran, G., Stolle, Dieter F.E., Horvath, Robert G. (2001) An investigation of scaling and dimensional analysis of axially loaded piles. *Canadian Geotechnical Journal*, 38(3), 530–541. https://doi.org/10.1139/t00-122

Setyaningrum, D.J., Amalia, D., Yuswandono, M., Sihombing, A.V.R., Septian, R., Yulianto, F.E. (2024) The effect of adding biopolymers on the physical properties of peat soils. *E3S Web of Conferences*, 479, 06004. https://doi.org/10.1051/e3sconf/202447906004

Shahrour, I., Rezaie, (1997) An elastoplastic constitutive relation for the soil-structure interface under cyclic loading. *Computers and Geotechnics*, 21(1), 21–39. https://doi.org/10.1016/S0266-352X(97)00001-3

Shinde, B., Sangale, A., Pranita, M., Sanagle, J., Roham, C. (2024) Utilization of waste materials for soil stabilization: A comprehensive review. *Progress in Engineering Science*, 1(2–3), 100009. https://doi.org/10.1016/j.pes.2024.100009

Singh, A.P., Rao, K.S., Ayothiraman, R. (2024) Model testing of rock-socketed piles under combined vertical-lateral loading. *Geotechnical Testing Journal*, 47(2), 539–562. https://doi.org/10.1520/GTJ20220173

Smith, L., Stark, N., Jaber, R. (2023) Relating side scan sonar backscatter data to geotechnical properties for the investigation of surficial seabed sediments. *Geo-Marine Letters*, 43(2), 9. https://doi.org/10.1007/s00367-023-00750-5

Tang, X., Yu, J., Wang, H., Kumar, A., Wang, M., Kattel, G.R., Han, L., Lin, J., Yu, Z.G. (2024)

Unravelling substrate availability and redox interactions on methane production in peat soils of China. *European Journal of Soil Science*, 75(1), e13456. https://doi.org/10.1111/ejss.13456

Ulusay, R., Tuncay, E., Hasancebi, N. (2010) Geo-engineering properties and settlement of peaty soils at an industrial site (Turkey). *Bulletin of Engineering Geology and the Environment*, 69, 397–410. https://doi.org/10.1007/s10064-010-0290-2

Vakili, A.H., Khajeh, A., Shalchian, M.M., Tajari, R. (2025) Experimental analysis of parameters affecting the lateral resistance of micropile groups embedded in sandy soil. *Results in Engineering*, 27, 105663. https://doi.org/10.1016/j.rineng.2025.105663

Venkatramaiah, C. (2006) *Geotechnical Engineering*. Revised third edition, New Age International, New Delhi IN, 926 pp.

Wang, Z., Zhou, H., Sheil, B., Liu, H., Wang, C. (2023) Numerical investigation of the lateral response of pile groups in sand under local scour conditions. *Computers and Geotechnics*, 159, 105435. https://doi.org/10.1016/j.compgeo.2023.105435

Wen, Y., Wang, S., Mu, W., Yang, W., Jönsson, P.G. (2020) Pyrolysis performance of peat moss: A simultaneous in-situ thermal analysis and bench-scale experimental study. *Fuel*, 277, 118173. https://doi.org/10.1016/j.fuel.2020.118173

Williams-Mounsey, J., Grayson, R., Crowle, A., Holden, J. (2021) A review of the effects of vehicular access roads on peatland ecohydrological processes. *Earth-Science Reviews*, 214, 103528. https://doi.org/10.1016/j.earscirev.2021.103528

Wilson, M.P. (2025) Monitoring peatland condition and restoration sites using vertical surface motion data from the European ground motion service. *Journal of Geophysical Research: Biogeosciences*, 130(2), e2024JG008670. https://doi.org/10.1029/2024JG008670

Wüst, R.A., Jacobsen, G.E., von der Gaast, H., Smith, A.M., (2008) Comparison of radiocarbon ages from different organic fractions in tropical peat cores: insights from Kalimantan, Indonesia. *Radiocarbon*, 50(3), 359–372. https://doi.org/10.1017/S0033822200053492

Yamazoe, N., Tanaka, H., Ogino, T., Nishimura, S. (2023) Mechanism of sampling disturbance for peat ground and its influence on mechanical properties. *Soils and Foundations*, 63(5), 101361. https://doi.org/10.1016/j.sandf.2023.101361

Yamazoe, N., Nishimura, S., Tanaka, H., Ogino, T., Kochi, T. (2025) Long-term settlement behavior of peat after unloading and applicability of isotach law. *Soils and Foundations*, 65(1), 101560. https://doi.org/10.1016/j.sandf.2024.101560

Yang, Q., Liu, Z., Bai, E. (2023) Comparison of carbon and nitrogen accumulation rate between bog and fen phases in a pristine peatland with the fen–bog transition. *Global Change Biology*, 29(22), 6350–6366. https://doi.org/10.1111/gcb.16915

Yonebayashi, K., Okazaki, M., Pechayapisit, J., Vijarnsorn, P., Zahari, A.B., Kyuma, K. (1994) Distribution of heavy metals among different bonding forms in tropical peat soils. *Soil Science and Plant Nutrition*, 40(3), 425–434. https://doi.org/10.1080/00380768.1994.10413320

Zainorabidin, A., Zolkefle, S.N.A., Basri, K., Mohamad, H.M., An, K., Ang, A.S., Hasan, M.F.R., Agung, P.A.M. (2023) Correlations of the dynamic parameters on Malaysia hemic peat. *Journal of Advanced Research in Applied Mechanics*, 124(1), 141–151. https://doi.org/10.37934/aram.124.1.141151

Zainorabidin, A., Zolkefle, S.N.A., Basri, K., Mohamad, H.M., An, K., Ang, A.S., Hasan, M.F.R., Agung, P.A.M. (2024) Correlations of the dynamic parameters on Malaysia hemic peat. *Journal of Advanced Research in Applied Mechanics*, 124(1), 141–151. https://doi.org/10.37934/aram.124.1.141151

Zhang, D., Zhang, X., Tang, H., Zhao, Z., Guo, J. and Zhao, H. (2023) Effects of soil arching on behavior of composite pile supporting foundation pit. *Computational Particle Mechanics*, 10(3), 645–662. https://doi.org/10.1007/s40571-022-00518-1

Zhang, A., Li, X., Zhou, W., Wang, W. (2025) Application research of miniature group pile foundation in a 500kV power transmission project. In: *Proceedings of the 2024 7th International Conference on Civil Architecture, Hydropower and Engineering Management (CAHEM 2024)*, Atlantis Press (Springer Nature), Dordrecht NL, 75–80. https://doi.org/10.2991/978-94-6463-650-5_8

Zimar, A.M.Z., Nasvi, M.C.M., Jayakody, S. (2020) Geotechnical characterization of peats in Muthurajawela Region in the Western Coast of Sri Lanka. *Geotechnical and Geological Engineering*, 38, 6679–6693. https://doi.org/10.1007/s10706-020-01462-8

Submitted 18 Mar 2025, final revision 15 Nov 2025
Editor: Gerald Jurasinski

Author for correspondence: Dr Rajat Debnath, Institute Post-Doctoral Fellow, Department of Civil Engineering, National Institute of Technology, Silchar, India. Tel: +91 7005287177; E-mail: rd2100@gmail.com

Appendix

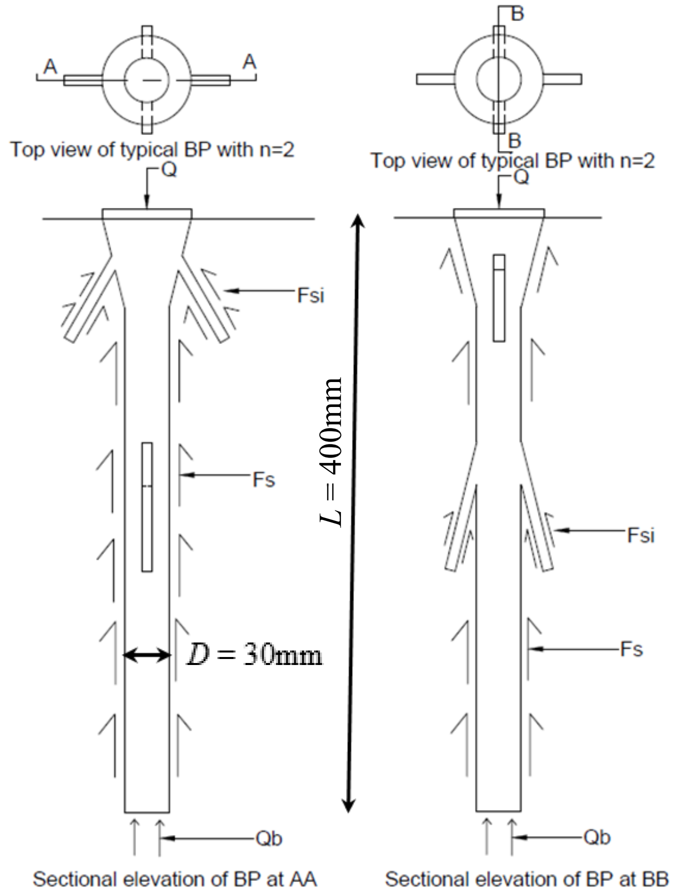

KEY

Df:: diameter of top portion of pile forming a cone shaped frustum.

Hf: height of of cone shaped frustum at upper end of the pile.

Db: diameter of branches.

Ltb: length of top branches inclined at an angle of α to vertical.

Lbb: length of bottom branches inclined at an angle of β to vertical.

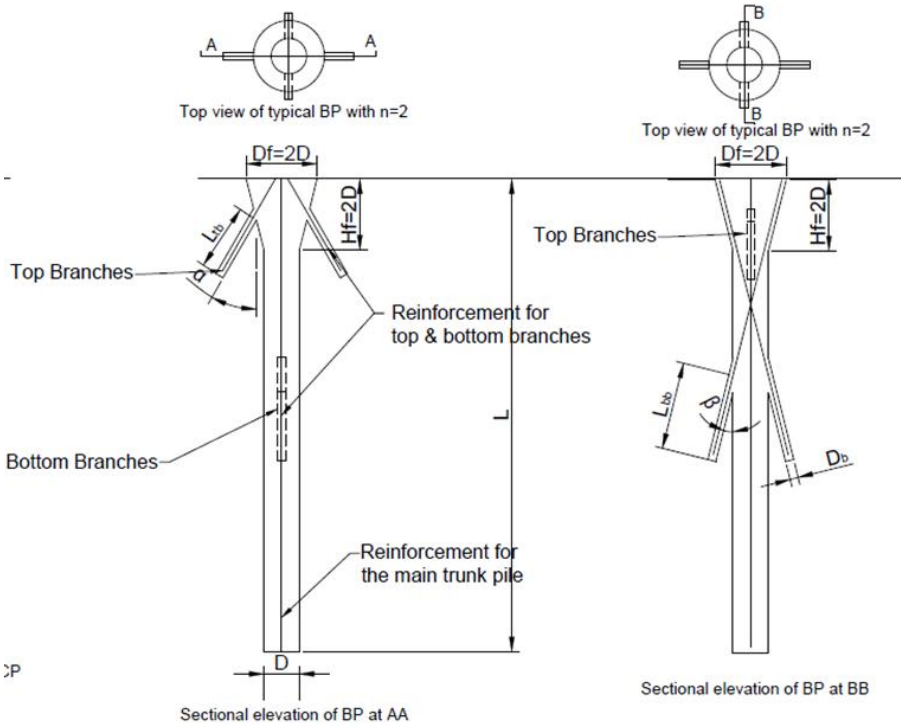

Figure A1. (a) Schematic diagrams of branched piles (BP) showing various dimensions including length of pile (L), diameter of pile (D) and branch length (Lb); see the key for further details.

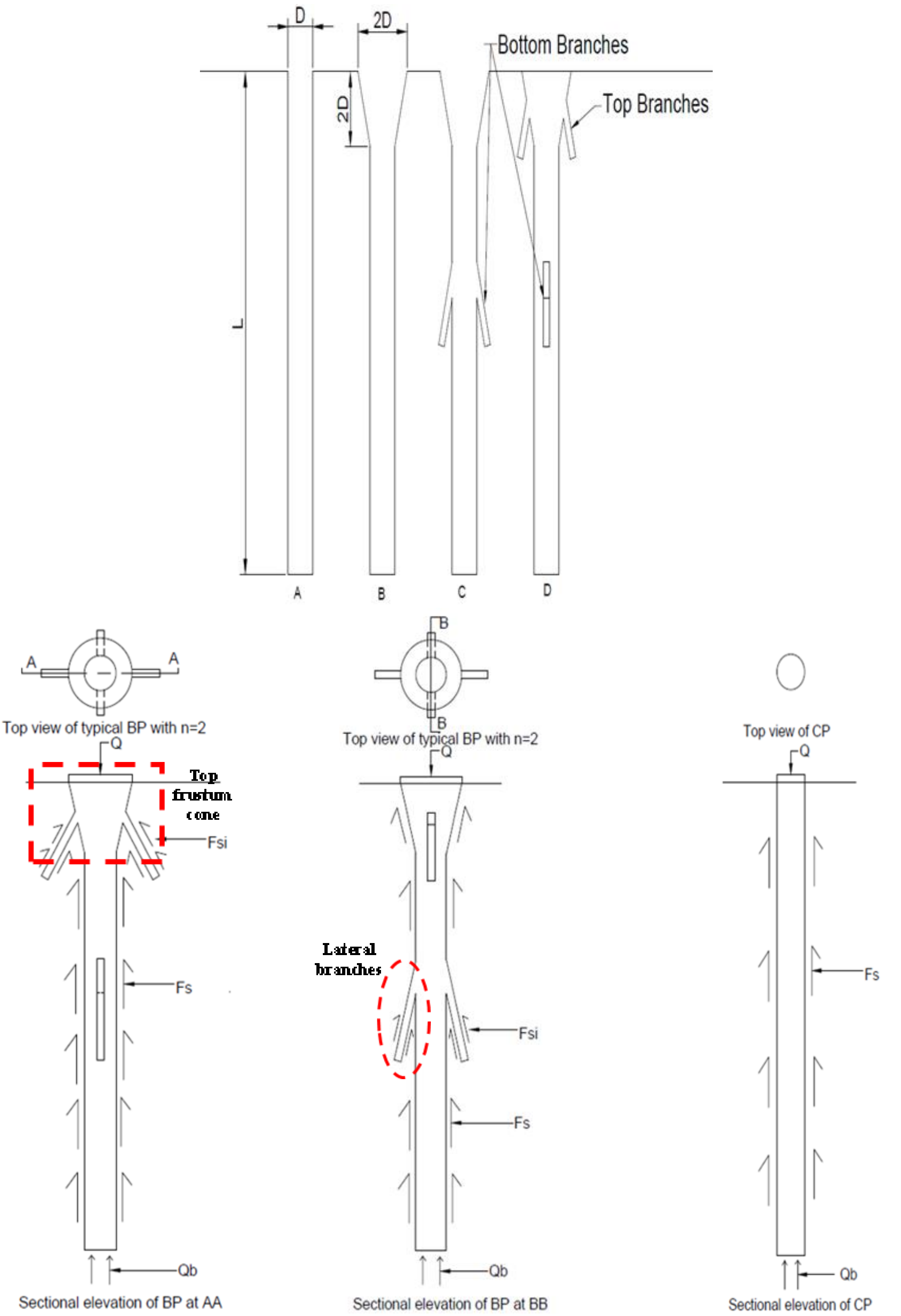

Figure A2. Top: concept sketches illustrating steps in BP installation. These are, from left to right: creation of a vertical borehole to accommodate the main shaft of the pile; formation of the top frustrum cone; drilling of inclined boreholes for the bottom whorl of branches; and finally, drilling of inclined boreholes for the top branches. Bottom: sketches comparing the structures of a branched pile (BP; left and middle) and a conventional pile (CP; right), highlighting the integrated top frustrum cone and lateral branches of the BP.

Table A1. Properties of the cement slurry used for preparation of piles.

Properties	Values
Normal consistency	29 %
Soundness	7 mm
Initial setting time	30 minutes
Final setting time	600 minutes
Compressive strength (3 days)	24.9 MPa
Compressive strength (7 days)	36.2 MPa
Specific gravity	3.13

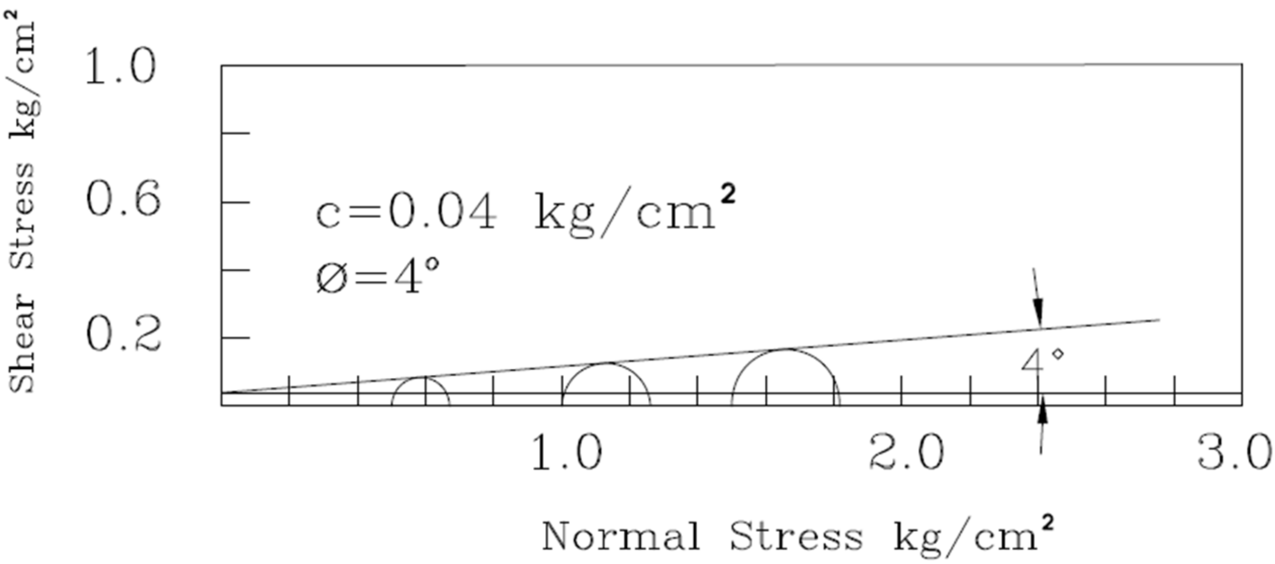

Figure A3. Strength parameters derived in the form of cohesion (c) and angle of internal friction (ϕ) from triaxial test.

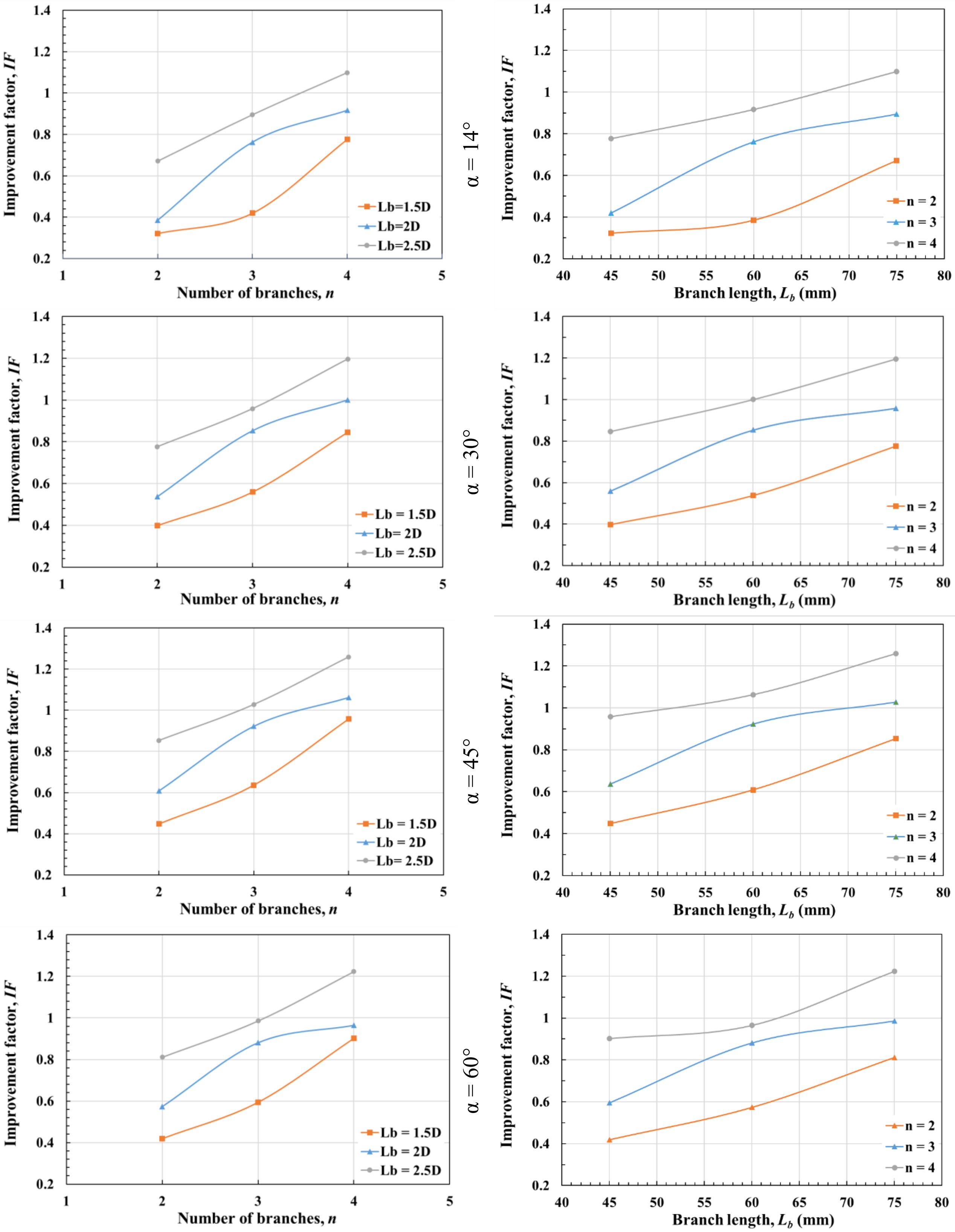

Figure A4. Effect on improvement factor (*IF*) of number of branches (*n*; left-hand column) in scenarios with L_b constant (per plotted line) and top branch inclination (*α*) constant (per panel); and of length of branches (L_b; right-hand column) in scenarios with *n* constant (per plotted line) and top branch inclination (*α*) constant (per panel).

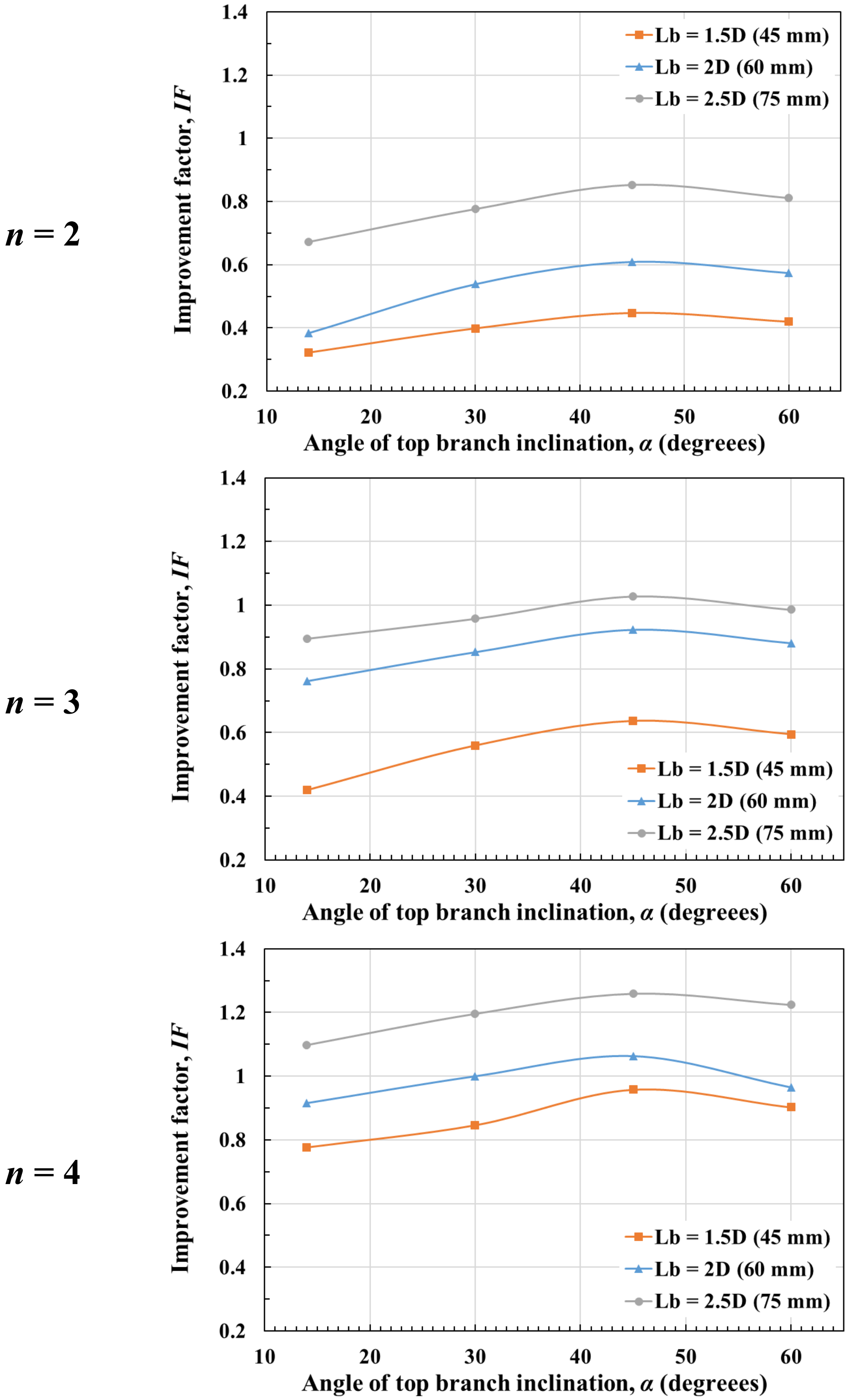

Figure A5. Effect of varying top branch inclination (α) on improvement factor (*IF*), in scenarios with length of branches (L_b) constant (per plotted line) and number of branches (n) constant (per panel).